I would like to thank the two Referees for their comments. Our manuscript benefited a lot from their suggestions and we hope to convince them with the revised version of the manuscript.

This document contains the detailed responses to Referee#1 and Referee#2 as submitted on the 21 Oct 2020, as well as a marked-up version of the revised manuscript (starting on page 21).

Best Regards,

Josefine Herrford

Answers to Referee #1

We would like to sincerely thank Referee #1 for their thoughtful comments improving our manuscript, as well as, the time and effort they put into this review. Below we address all issues raised in this review by responding to the individual comments, corrections and suggestions in italic.

General Comments

The study of the seasonal variability of the Atlantic Meridional Overturning Circulation (AMOC) at 11S is very important, however, some aspects of this study need clarification to warrant its publication in Ocean Science.

While any effort to extract as much information about the AMOC variability as possible from temporally and spatially sparse existent data is appreciated, the use of a model simulation (1948-2007) that does not overlap with the observations (2013-2018) is problematic. This makes it harder to pinpoint the reasons for the differences between model and observations and thus to trust the chosen observational strategy. As a consequence, the seasonal cycle of AMOC transport from the observations is very different from that obtained from the model. Not only the maximum and minimum values occur in different months of the year, but also their amplitudes are statistically different.

This is correct. Comparing two different periods does not allow us to analyze the correspondence of interannual variations in observations and simulations. Differences between model and observations are thus partly the result of the different periods analyzed. Unfortunately, at the moment, there is no suitable model run with atmospheric forcing covering the observed period (e.g. JRA55-do) available and sufficiently validated. However, the model is very well suited to analyze general aspects of the seasonal cycle and particularly the uncertainties of our method to derive the seasonal cycle of an AMOC time series from observations: Similar concepts are followed in Observing System Simulation Experiments (e.g. Gasparin et al., 2019; https://www.frontiersin.org/articles/10.3389/fmars.2019.00083/full).

In addition, the description of the results using different periods of time is very confusing. For instance, the periodograms of Ekman transport are presented for 2013-2018 from ASCAT dataset and for 2002-2007 from CORE2b dataset. But the minimum and maximum ranges are calculated from ASCAT for 1993-2018 and from CORE2b for 1978-2009. Even though the two datasets overlap for the period of 1993-2009, the authors then show the Hovmöller of zonal wind stress for 2008-2009. It is not clear why this is done. It would be better to compare the wind seasonal cycle obtained from both datasets for the period of 1993-2009.

We are sorry, we made a mistake here. ASCAT wind stress is available for the period 03/2007-12/2018, not 1993-2018. These numbers are corrected in the revised manuscript. When we first analyzed the model, the INALT01 model run covered the period 1978-2007. But since the CORE 2b forcing data set covers 2 more years (1978-2009), a direct comparison of ASCAT and CORE 2b wind stress in 2008-2009 (overlapping full years) is possible and performed.

In figure 7a, we show a periodogram of wind stress calculated for 5 years (2013-2018), for which BP measurements are available. As ASCAT covers a longer period, we can also provide an estimate for interannual variations ("minimum and maximum ranges of periodograms calculated for 5-year windows running through the full time series") plotted as an envelope. In figure 7b for CORE 2b wind stress, the 5-year period 2002-2007 was chosen arbitrarily. We understand, that this is confusing. In the revised manuscript, we do only show the envelope representing the interannual range of periodograms calculated for different 5-year subsets of the full time series.

Finally, the manuscript is long and most of its content is on validating the analysis rather than showing and discussing the main results about the AMOC variability. For instance, the latter is only introduced on page 11. The readability of the manuscript would also improve if information is conveyed in a more clear and straightforward way.

We think that the results of this study benefit from a comprehensive validation of the analysis. In order to improve the readability, we tried to go through the manuscript sentence by sentence, streamline and shorten the text as much as possible.

Specific Comments

Lines 21-22: "Here, long Rossby waves originating from equatorial forcing are known to be radiated from the Angolan continental slope and propagate westward into the basin interior." Is this shown in this study (here) or concluded from other studies? After reading the manuscript, I could not find any analysis that presents this.

This is concluded from other studies. In the abstract, we deleted this sentence. In other paragraphs we included Kopte et al. (2018) as the reference in which the westward propagation is discussed as part of an equatorial basin mode (see also Brandt et al., 2016):

Lines 103-158: Sub-sections 1.1, 1.2, 1.3 and 1.4 should be 2.1, 2.2, 2.3 and 2.4, respectively.

Corrected.

Line 116: I am not sure if it is necessary to describe the software used to calculate the tidal harmonics.

We would like to keep the reference, but removed the description of the software.

Lines 120-121, 133-134: Fig. 2a and Fig. 2b should be Fig. 1a and Fig. 1b, respectively.

Corrected.

Lines 200-205: Did the authors test other depths to have an estimate of the sensitivity of this choice (z=1130m)?

Yes, we did. In our study, we defined our level of no motion based on the mean depth of the zero-crossing of the meridional velocity along 11°S in the INALT01 model. And, indeed, at 11°S this depth is more variable than, for example, at 26.5°N. Most of the time (for 87% of the timesteps) this depth varies between 800m and 1300m depth, mainly following a seasonal cycle. Varying the level of no motion within this range changes the mean AMOC transport, which is largest when integrating to 1130m (14.1 Sv), by less than 10% (see Fig. 1 R1; upper panel). We added a sentence regarding this sensitivity to section 4.1. The peak-to-peak amplitude of the mean seasonal cycle of the AMOC decreases with depth – from 7.2 Sv at ~730m to 5.6 Sv at ~1470m and its minimum shifts from October to August (see Fig. 1 R1; lower panel). This is probably due to including parts of the southward lower branch when integrating to deeper levels. We added a sentence to section 4.1

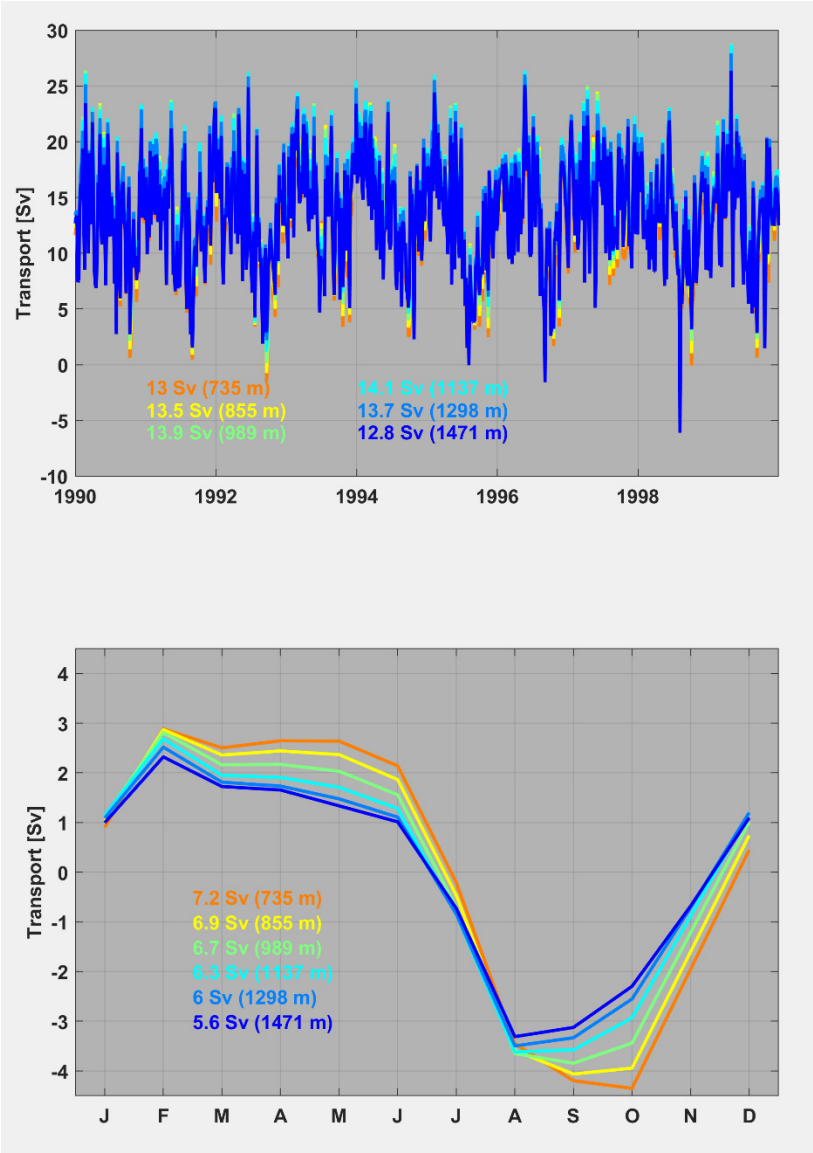

Figure 1 *AMOC transport timeseries (5-daily; upper panel) and mean seasonal cycle (lower panel) at 11°S derived from the INALT01 model velocity fields over the period 1978-2007. Different colors denote different choices of a 'level of no motion' for the integration.*

Lines 280-283 & Fig. 4: Which of these peaks are statistically significant? Particularly, considering the annual and semi-annual harmonics from 2-year long time series. This is different from the calculated uncertainty shown in shading.

We tested if the peaks in the periodograms of the BP time series are significant against the red noise background from an AR1 process (see Fig.2 R1; black solid curves are AR1-95%-confidence bounds and black dashed curves AR1-68%-confidence bounds). The annual cycles in the 2-year long BP time series off Angola are the only significant peaks against the 95%-confidence range of an AR1 process. When considering the 68%-confidence range then the peaks of the semi-annual cycles of Angola and at the western boundary at 500m are also statistically significant.

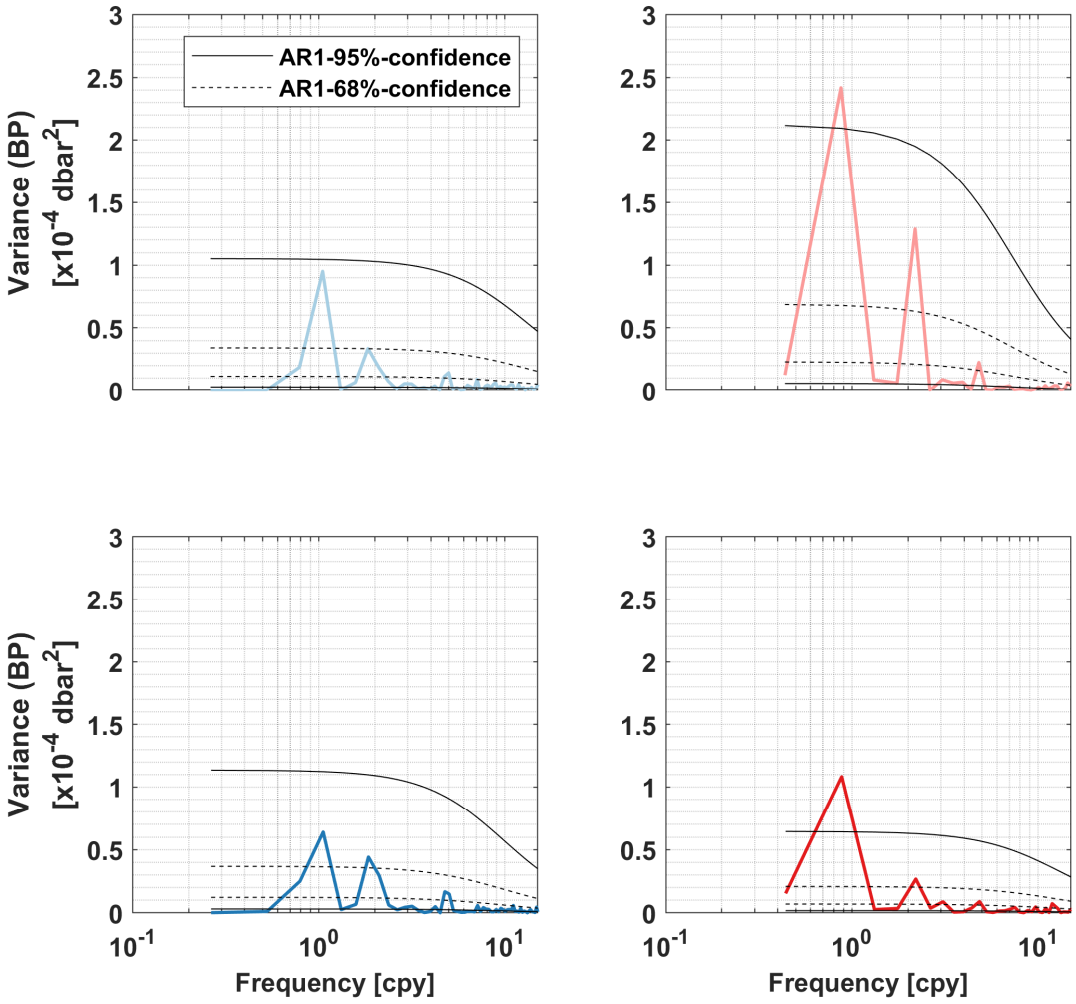

Figure 2 *Similar to Fig.4 in the manuscript. Periodograms of BP at 300 m (upper panels) and BP at 500 m (lower panels) depth at the western (left panels) and eastern (right panels) boundaries at 11°S - calculated over the period 2013-2018. Black curves are the 95%-confidence (solid) & 68%-confidence (68%) ranges of an AR1 process.*

Lines 297-298: Isn't this also related to the fact that the observed time series are very short and cannot capture well the annual harmonic?

In INALT01, we are able to test how our results are affected by interannual variations and different time series lengths. Typically, we show the possible range of spectra, harmonics or mean seasonal cycles calculated for different 5-year subsets of the 30-year model run, but we also tested how the seasonal harmonics change using for example 1-year subsets, thus the total amount of available seasonal cycles of the model run and the shortest possible time series length. However, we obtain the robust result that, in INALT01, the amplitudes of the annual and semi-annual harmonics at 300m and 500m depth, and especially at the western boundary, are systematically underestimated compared to the observations.

Lines 309-311: Why is the periodogram for the CORE2b wind stress calculated for 2002-2007? Could a longer period from the model data be used as well to assess the impact of such observed short time series on the variability?

As our observational period covers about 5-years, we wanted to also show the periodogram for an arbitrary 5-year period of the CORE2b timeseries. However, the transparent envelopes, which are supposed to represent interannual variations of the results, already show the minimum and maximum ranges of periodograms calculated for 5-year windows running through the full available time series of

CORE2b (1978-2009) - including the subset 2002-2007. From the comments we understand, that this was rather confusing than helpful. We deleted the solid curve in Fig. 7b and tried to modify the related text and figure caption in the revised version accordingly.

Lines 310-311: "The CORE2b winds do also show weak semi-annual variability, but only when considering the full time series from 1978-2009", where is this shown?

In Fig. 7b, the transparent envelope representing interannual variations shows a second, smaller peak at a frequency of 180 days. As this peak is not statistically significant we deleted this sentence in the revised manuscript.

Lines 311-322: Perhaps, it would help to show an extra panel similar to panels Fig. 7c,d with the climatological evolution obtained from both dataset for 1993-2009. In fact, it is very confusing, the model outputs are for the period of 1978-2007 (Section 3). The Ekman transport periodograms are obtained from ASCAT for 2013-2018 and from CORE2b for 2002-2007. But the minimum and maximum ranges are calculated for the 1993-2018 for ASCAT and 1978-2009 for CORE2b. Why not to show a climatological Hovmöller for the overlapping period 1993-2009, instead of for 2008-2009?

We are sorry for the confusion, which, we think, is mainly caused by a mistake we made in the caption of Fig. 7. ASCAT wind stress is available for the period 03/2007-12/2018, not 1993-2018. The INALT01 model run covers the period 1978-2007. But since the CORE 2b forcing data set covers 2 more years (1978-2009), a direct comparison of ASCAT and CORE 2b wind stress in 2008-2009 (overlapping full years) was possible and performed.

Lines 336-338: The seasonal cycles of TAMOC from the observations and model are not similar. In particular, the maximum observed TAMOC occurs in May and the maximum modeled TAMOC in February, whereas the minimum observed TAMOC occurs in October and minimum modeled TAMOC in August. The amplitudes are also statistically different, comparing the error bars for the observations with the shading for the model.

This is correct. In the revised manuscript, in addition to the minimum and maximum ranges of mean seasonal cycles calculated for running 5-year windows running through the respective available periods we do also show the total range of possible values per month. Even when considering the total range, the mean seasonal cycles of T'_G and T'_{AMOC} are just outside the total range of possible results in INALT01. We rephrased several related sentences and tried to be more specific on where we find good agreement and where we find differences. However, we think that the model is very well suited to analyze the relevant mechanisms and test our method to derive the seasonal cycle of an AMOC time series from observations.

Lines 359-360: This is not the case for TAMOC (previous comment).

Please see the previous comment.

Lines 376-389: It seems that the observation/model comparison is inconclusive.

We now more clearly state where we find good agreement and where we find differences between model simulations and observations (see above).

Lines 395-403: In Fig. 12, why is the slice from 15W to 5W not included in the calculation for the interior transport? The definition of AMOC transport encompasses the whole basin, and if one wants to discuss the contributions of the WBC, interior and EBC to the AMOC variability, the slice from 15W to 5W has to be included in the interior transport. Later in lines 418-420, the authors state that there is a minimum in the annual and semi-annual harmonics in this range. However, this is not a good reason to not include the contribution from 15W-5W in the calculations. If the related transport is

also minimum there, including this won't affect the main findings, but it will make the results more consistent.

This is absolutely right. We extended the slices of the Western basin Interior and eastern basin to 10°W, which corresponds approximately with the location of the Mid-Atlantic Ridge crest. The results change very little. The minimum of the seasonal cycle of the eastern basin contribution, however, is reduced by half its amplitude and shifted from September to August. A small maximum in February is gone. Extending the eastern basin slice to 10°W results in an even greater similarity between its seasonal cycle and the seasonal cycle of the basin-wide upper-ocean geostrophic transport.

Line 401-403: This is why the use of a model output that encompass the same period of the observations is so important. And also, a comparison between using shorter versus longer time series from model outputs would permit to evaluate the impact of using observed short time series on the seasonal variability.

As stated above, at the moment, there is no suitable model run with atmospheric forcing covering the observed period (e.g. JRA55-do) available and sufficiently validated. We hope for this to happen in the near future. In order to give an estimate for possible interannual variations, all mean seasonal cycles are shown together with the total range of possible values (single years) and, for the 30-year model run, the range calculated for 5-year subsets. We tried to highlight this more clearly in the text.

Lines 401-427: Fig. 13a is not mentioned in the text but shows that there is not a defined seasonal cycle of the NBUC during the period of 2013-2018.

Fig 13a is now mentioned in section 2.4. Despite the large year-to-year variability in the seasonal cycle, a mean seasonal cycle can be obtained (shown in Fig. 13b) that can be compared to a mean seasonal cycle and its variability as obtained from the model simulations.

Lines 428-531: What is the impact of using the combined annual and semi-annual cycles for the eastern boundary after 11/2015 since they explain 44-61% of the variance in the daily BP time series there and for the western boundary before 05/2014 since they explain only 18-24% of the variance in this case (Lines 229-238). This was one of the main reasons to use the model outputs. Doesn't this procedure lead inevitably to the conclusion that the geostrophic transport variations are dominated by seasonal variability (Lines 466-467).

We tested replacing certain BPRs with the corresponding combined annual and semi-annual harmonics in the fully equipped period 05/2014 - 11/2015 (cf. Fig.8a). In those 18 months, the correlation between the daily T'_{G} time series derived with 4 BPRs ("$T'_{G\ EOFs\ 4\ BPRs}$") and the daily T'_{G} time series with the WB 300m BPR replaced ("$T'_{G\ EOFs\ 3\ BPRs}$") is high R=0.97 and the correlation with T'_{G} derived with 2 WB BPRs and the EB combined annual and semi-annual harmonics ("$T'_{G\ EOFs\ 2\ BPRs}$") is R=0.85. As the latter can explain ~70% of the total variance in T'_{G} over the fully equipped period, we are still confident to capture most of the variability in T'_{G} after 11/2015. As this period is only 18 months, we assume the 30% of the variance that we seem to miss with our method to be related to the intra-seasonal signals we see in the spectra for EB BP (Fig.4 d, f). However, it is correct, that with our methods we give too much weight to seasonal variability compared to other timescales, but on the other hand we believe it is the best we can make out of the currently available time series.

Having measurements only at 2 depths and the surface, the main reason to use the model, was to understand and approximate the vertical structure of V'_{G} (z). We do not use the model to fill data gaps or replace missing sensors.

Lines 428-531: This section is too long, and the manuscript readability would benefit if most of this discussion was made in Section 5 when the authors present the results. It is difficult to go back to

figures and description of the results at this point to verify, for instance, that the structure of the meridional geostrophic velocity in the eastern basin is linked to CTW. Is this really shown in the results?

We tried to shorten this section as much as possible and shifted parts of the discussion to section 5. In the manuscript, we also tried to clarify, that only the vertical structure and variability of the pressure at the eastern boundary can be related to CTWs – not the vertical structure of the meridional geostrophic velocity integrated over the whole eastern basin.

Minor Comments

Line 254: "We also test or: : :" should be "We also test our: : :"

Corrected. Thanks.

Line 305: In "Prevailing wind stress along 11S is northwestward: : :", consider instead: "The prevailing winds along 11S are from southeast: : :".

We changed the sentences accordingly.

Line 325-326: To improve readability, consider "Figure 8 displays the derived time series of TG, TEK, and the sum of both components TAMOC at 11S." instead of "Figure 8 displays the derived time series of TG, TEK, and being the sum of both components, TAMOC at 11S."

Changed.

Line 412: ": : : to cancel out each other: : :" should be ": : : to cancel each other out: : :"

Corrected.

Line 460: "und" should be "and".

Corrected.

Line 752: "Hovmoeller" should be "Hovmöller"?

Corrected.

References

Brandt, P., Claus, M., Greatbatch, R. J., Kopte, R., Toole, J. M., Johns, W. E., and Böning, C. W.: Annual and semiannual cycle of equatorial Atlantic circulation associated with basinmode resonance. J. Phys. Oceanogr., 46, 3011–3029, https://doi.org/10.1175/JPO-D-15-0248.1, 2016.

Gasparin, F., Guinehut, S., Mao, C., Mirouze, I., Rémy, E., King, RR., Hamon, M., Reid, R., Storto, A., Le Traon, P-Y., Martin, M.J. and Masina, S.: Requirements for an integrated in situ Atlantic Ocean observing system from coordinated observing system simulation experiments. Front. Mar. Sci., 6, 83, https://doi.org/10.3389/fmars.2019.00083, 2019.

Answers to Referee #2

This is a very nice study producing for the first time an estimate of the seasonal cycle of the meridional overturning circulation in the tropical South Atlantic along 11S using a few bottom pressure measurements (BPRs and PIES) on the boundary, satellite winds, sea level from altimetry, as well as information provided from a model (INALT01). I think that this paper reads well and the analysis presented here is important. The authors make innovative use of a few moorings to reconstruct the AMOC volume transport time series.

We would like to sincerely thank this referee for their kind words, the time and effort they put into this review and the helpful suggestions improving our manuscript. Below we address the issues raised in this review by responding to the individual comments from Referee #2 in italic.

General comments:

1. I don't get a sense from the manuscript, how the amplitudes for AMOC seasonal cycle transports documented at 11S compare with those at other latitudes (i.e., 26N and 34.5S) from previous studies. There is recent some evidence from observations that AMOC amplitudes decrease northward of 34.5S (i.e., Dong et al., 2015; Frajka- Williams et al. 2019; Kersale et al., 2020), and it would be nice to know how your results fit into the context of previous studies.

As seasonal AMOC variability is closely related to variations in the regional wind regimes, we do not expect similar amplitudes or phases of the seasonal cycle of the AMOC in the Tropics compared to the Subtropics or Subpolar regions. Therefore, comparing our results directly to the seasonal cycle of the AMOC observed at RAPID or SAMBA does not seem to be extremely useful with regard to the local mechanisms, but indicate the importance of understanding the seasonal cycle when trying to extract longer-term variability from observations. Thus, we added a list of the seasonal cycle amplitudes of the AMOC at RAPID and SAMBA to the discussion: "In the Subtropics, recent estimates of the peak-to-peak amplitude of the mean seasonal cycle of the AMOC range from 4.3 Sv at 26.5°N (2004-2017; Frajka-Williams et al., 2019) to 13 Sv at 34.5°S (2014-2017; Kersale et al., 2020)." Thank you for pointing out the study by Kersale et al. (2020) – we had not been aware of it. The seasonal cycle of the AMOC at 11°S is similar in amplitude compared to SAMBA and much stronger than at RAPID.

2. It is unclear when you report a mean +/- number whether that second number is the standard deviation, the standard error, or the uncertainty. If it is the standard error or the uncertainty, some explanation is needed for how you got to that number (i.e., how many degrees of freedom did you assume).

In the submitted manuscript, all error bars plotted together with mean seasonal cycles (fig.9 (a,c,e) and fig.13 b) were standard errors $\left(=\frac{\sigma}{\sqrt{N}}\right)$ *with σ being the standard deviations and N the number of available years. In the revised version of the manuscript – as a response to other comments - we show the absolute range of possible values as dashed curves instead.*

In the text, the "±"-numbers provided together with estimates of mean transports are also standard errors $(=\frac{\sigma}{\sqrt{M_{eff}}})$ *, but with* $M_{eff}=\frac{M}{n_d}$ *, where M is defined as the length of the time series and* n_d *as the decorrelation time scale. To clarify this, we added a sentence to the methods ("In the following, all mean transports are presented together with the standard error* $SE=\sigma/\sqrt{N/n_d}$*, where σ is the standard deviation and nd the decorrelation time scale of the respective time series of length N.") and changed a sentence in section 5.3 to "This is within the uncertainty range of 3 Sv for the AMOC estimate of 16.2 Sv derived from a hydrographic ship section along 11° S in 1994 (Lumpkin & Speer, 2007)."*

3. Assuming those numbers are standard deviation or standard error, that represents the variability in the time series, not the uncertainty associated with your measurement strategy. Have you made a qualitative estimate of the measurement uncertainty for each daily estimate (i.e., examined the sources of error)? If so, what is that error?

Many problems associated with the measurements of the bottom pressure recorders, like the sensor drift or de-tiding, are thoroughly discussed in Kanzow et al. (2006). We followed their procedure and tried to document all the steps and choices we made during the processing of the BPRs. These are the uncertainties associated with the instruments themselves.

The second part of uncertainties arises from the observational strategy: With BP observations only at 2 depths and SLA at the surface, we had to test the uncertainties associated with this observing system and our methods to approximate the vertical structure of the basin-wide geostrophic transport above 1000m. To do this we use the INALT01 model. INALT01 was found to produce comparable variations in the Western Boundary Current transport at 11°S (Hummels et al., 2015) and, therefore, considered to be a good choice for this analysis. Of course, the model is not perfect. However, even if there are differences between the model and the reality, we can use the model "reality" to test our observational strategy meaning that with the help of the model, we were able to quantify uncertainties of the derived transports that are related to different aspects of the observing system.

That's why large parts of our manuscript are already very technical, as pointed out by Reviewer #1. We consider the effect of the uncertainty of each daily estimate on the seasonal variability of geostrophic transports small compared to the uncertainty introduced by the different aspects of the observing system, mainly because of the dominance of the annual and semi-annual variability compared to variability on other time scales.

4. The figures are really nice, however, some of the figure captions are hard for me to parse. I would suggest some streamlining of the figure caption text. Some of the colors used have names that are not familiar to everyone (i.e., petrol in Fig. 8,9 and elsewhere). The colors are fine, just the nomenclature is less common (to me) and may not be familiar to all.

We tried to streamline all of the figure captions as well as to simplify the color scheme and nomenclature.

5. What do you think is the uncertainty in your AMOC transport associated with not having information inshore of the 300m isobath? Did you examine this within the context of the model?

We tested this in the INALT01 model. There, the transport in the western boundary wedge inshore of the 300m isobath is -0.04 ± 0.002 Sv, hence negligible. And from velocity ship sections available along 11°S, we estimate even smaller transports between 0.007 -0.008 Sv for the 300m western boundary wedge.

6. One thing I was curious about is how much of the maximum northward volume transport (i.e., percent variance) does the Ekman vs. geostrophic volume transport account for in the observations and in the model? Do they have a very different breakdown? You talk about the amplitudes of each signal, so the result can possibly be inferred, but it is not explicitly stated in the manuscript.

Considering 5-year subsets of the 30 years of the INALT01 model run, the seasonal variability (repeated mean seasonal cycles) of $T_{EK\ CORE2b}$ can explain between 10-19% and $T_{G\ SIM}$ between 20-28% of the total variance in $T_{AMOC\ SIM}$. In the observations, which cover the years 2013-2018, seasonal variability of $T'_{EK\ ASCAT}$ and T'_{G} (using 5-day averages as in INALT01) can explain 13% and 48% of the total variance in T'_{AMOC}, respectively. This last number is, of course, strongly dependent on our method. Using the

combined annual and semi-annual harmonics whenever a sensor is missing results in over-weighting of seasonal variability while missing variability on other timescales.

7. Subsections of section 2 are labelled 1.1, 1.2, ... instead of 2.1, 2.2, : : :.

Corrected.

By line number:

21: When you say "long Rossby waves" do you mean annual Rossby waves? If so, the timescale should be mentioned at least once in abstract and in text.

This sentence was rephrased, but we modified this formulation whenever used elsewhere.

33-34: "downward and upward motion: : : Southern Ocean" – I find this part of the sentence hard to parse, I am not sure I understood it.

Changed to "……through water mass transformation, for example, in the subpolar North Atlantic or near the Southern Ocean."

48-55: A good summary paper for all of the international efforts that you may want to include if it is helpful is Frajka-Williams et al. (2019).

Indeed, it is a really good summary paper. We added this reference.

79: The "however" in this sentence doesn't seem needed as you are not making a contrasting statement.

Deleted.

85: Suggest "however they are also" instead of "but also to be"

Changed as suggested.

92: Imbol Koungue et al. (2017) may also be a useful reference here, but you already have several.

Thanks for the suggestion. We added the reference.

99: "can even more straightforward be estimated" is a little hard to parse

Changed to "But, circulation changes in z-coordinates can also be estimated by measuring the pressure differences between the eastern and western boundary at each depth."

120-121 and 133-134: You point to Figure 2 here but I believe you meant to point to Figure 1.

Corrected.

145: It is probably hard to estimate all of the uncertainties in your methodology/ measurement strategy, but the errors due to winds seem possible to estimate given that you are comparing two different wind products in your study. You already do this to some extent in talking about how it affects your results.

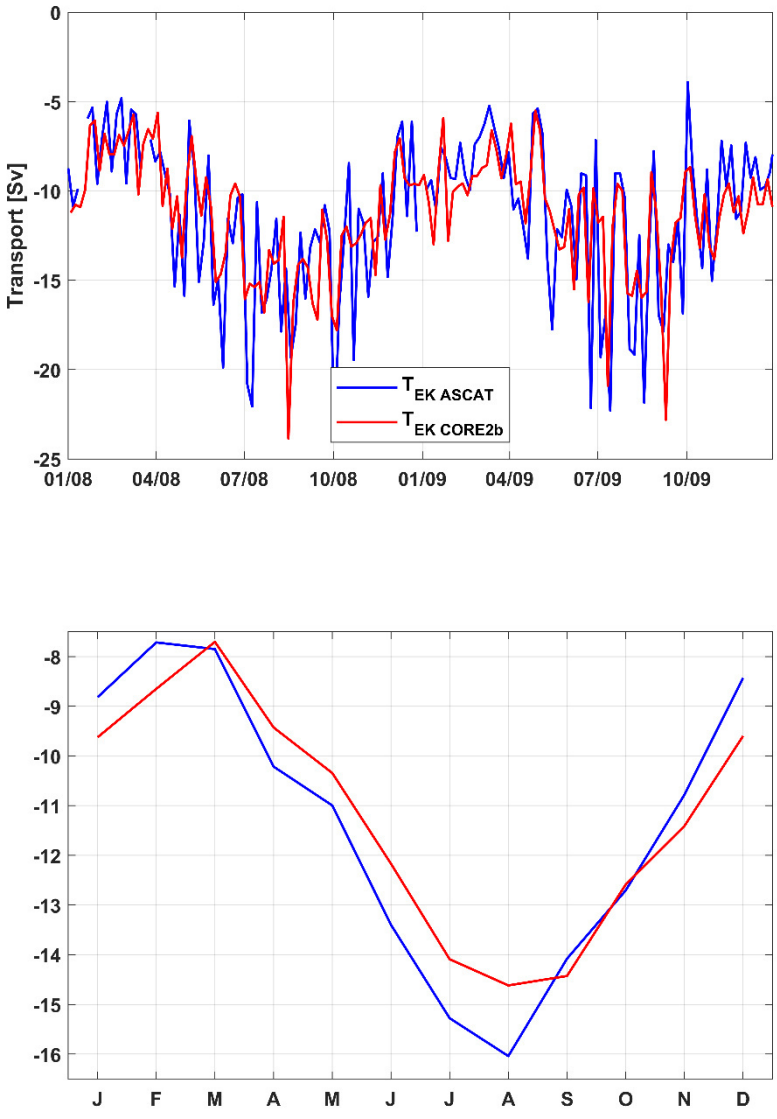

Figure 3 *Ekman transport time series (5-daily; upper panel) and mean seasonal cycles (lower panel) derived from ASCAT (blue) and CORE2b (red) wind stress for the overlapping years 2008-2009.*

In the manuscript we list the mean Ekman transports and standard errors for the two different products, we compare their respective periodograms and mean seasonal cycles together with estimate of interannual variations beyond the observational period. Additionally, Fig. 1 R2 (upper panel) shows the Ekman transport time series derived from 5-daily averages of ASCAT and 5-daily CORE2b wind stress for the overlapping years 2008-2009, which are highly correlated (R=0.82; upper panel). The mean seasonal cycles (Fig.1 R2; lower panel) calculated for the overlapping two years, show differences in amplitude and shifts up to 1 month between extrema. In comparison to the mean seasonal cycle we estimated for the upper-ocean geostrophic contribution to the AMOC seasonal cycle (cf. Fig. 9a in the manuscript), the differences between these two wind products – as estimated for 2008-2009 - are just within the uncertainty of the two methods we use to approximate the vertical structure of the geostrophic transport. We think that further investigations would be beyond the scope of this article.

151: Suggest "To estimate transports on the western boundary, we compute" instead of "We show"

Changed to "…To estimate the western boundary current transport, we compute....".

157: Suggest "These transports are computed following methodology of Schott et al. (2005) and Hummels et al. (2015) and represent updates from their previous transport time series" or something similar.

We re-arranged the paragraph, but would like to keep the information as the methodology is slightly different in Schott et al. (2005) and Hummels et al. (2015).

177: Shouldn't it be "from the western to the eastern boundary" in the parentheses?

Yes, correct. Thanks.

191-192: Here a reference to other studies in the South Atlantic may be beneficial (i.e., Meinen et al. 2018; Kersale et al. 2020).

As the methods between this study (using only the BPRs and SLA) are different the methods used to estimate the AMOC at SAMBA (travel time from PIES for "baroclinic" and BP for "barotropic" components), we think, adding these references here does not support the statement. However, we added Kersale et al. (2020) to the introduction when the efforts at SAMBA are introduced.

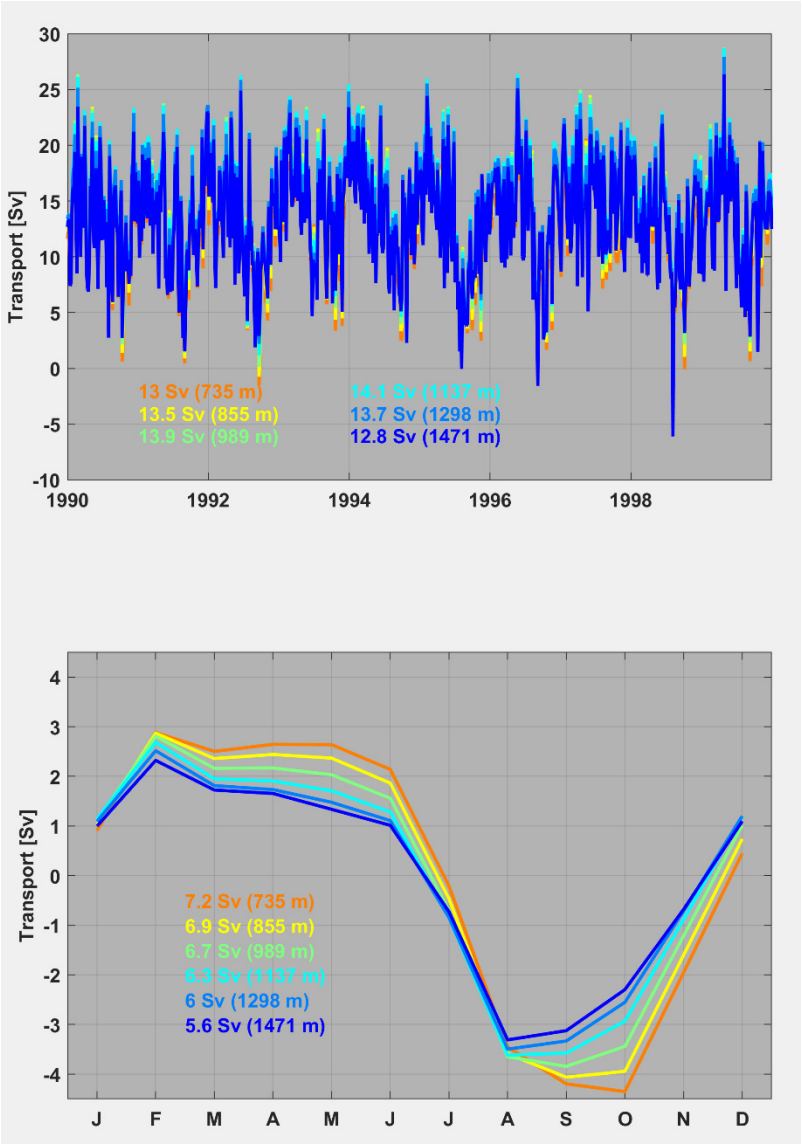

Figure 4 *AMOC transport timeseries (5-daily; upper panel) and mean seasonal cycle (lower panel) at 11°S derived from the INALT01 model velocity fields over the period 1978-2007. Different colors denote different choices of a 'level of no motion' for the integration.*

203: Are your results sensitive to your choice of 1130m as the mean depth of no motion? In the INALT01 model, how much did the depth of maximum overturning vary if you used 900m or 1300m for example?

Yes, they are, but within the range of the other methodological uncertainties. Indeed, at 11°S this depth of no motion is more variable than, for example, at 26.5°N. Most of the time (for 87% of the timesteps) it varies between 800m and 1300m depth, mainly following a seasonal cycle. Varying the level of no motion within this range (see Fig.2 R2; upper panel) changes the mean AMOC transport, which is largest when integrating to 1130m (14.1 Sv), by less than 10%. The peak-to-peak amplitude of the mean seasonal cycle (Fig.2 R2; lower panel) of the AMOC decreases with depth – from 7.2 Sv at ~730m to 5.6 Sv at ~1470m and its minimum shifts from October to August.

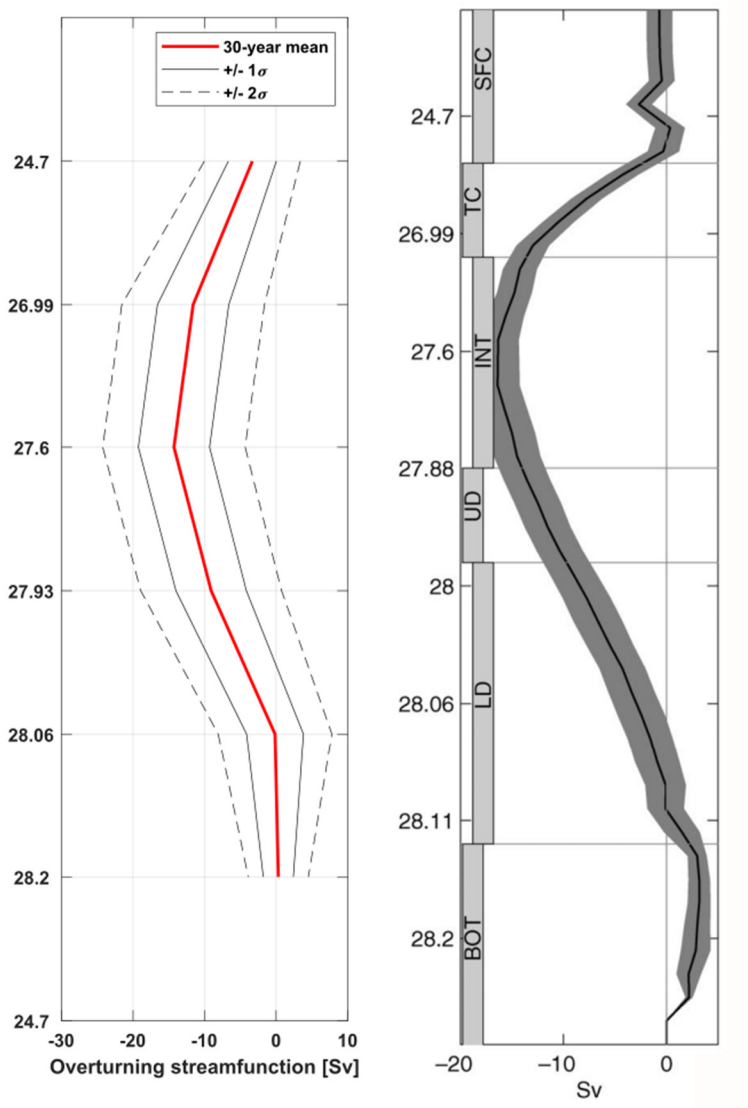

Figure 5 *Overturning streamfunction across 11°S with neutral density classes on the y-axis. Left panel: Derived from the INALT01 model velocity field over the period 1978-2007. Black curves give the one and two standard deviations around the 30-year mean. Right panel: Derived from the hydrographic WOCE sections A8 in 1994, copied directly from Lumpkin & Speer, 2003 (their Fig.8). The shading indicates standard error bars.*

209-213: I think you mention this in the paper, but some models don't have the right volume transport per unit depth structure (i.e., maxima is too shallow/narrow or too broad)? How well does INALT01's structure agree with the few hydrographic estimates of volume transport per unit depth that exist in the region? Maybe something to mention here or in Section 3 when model details are provided.

The only study we are aware of that presents an estimate of the overturning streamfunction at 11°S based on observations is by Lumpkin & Speer (2003, see Fig. 3 R2; right panel). They calculated their overturning streamfunction from the WOCE A8 section along 11°S conducted in 1994 and in defined neutral density classes. The results from INALT01 (Fig.3 R2; left panel) show good agreement regarding the vertical structure and ampitude of the overturning stream function when considering the range of possible variations around the mean over the 30-years of the model run. We added this information to section 3.

230: All of the other dates are month/year in the table, but here you have day/month/year. Suggest just using month/year.

Thanks. Corrected.

233-234: I know you don't have long enough records on eastern boundary to say how robust those%variance estimates are based on 2-years of data, but you could examine whether the % variance estimates on the western boundary are sensitive to using 2- vs. 4- years of data (i.e., look at % variance in the first two years, second two years, full record)

Thanks for the suggestion. We did: The table below lists the % of variances explained by the annual (AC), semi-annual (SAC) and combined harmonics fitted to 2-year subsets of the WB BPR timeseries.

We find the combined annual and semi-annual harmonics to always explain a similar fraction of the overall variance in the time series. But, the fractions related to the annual or semi-annual harmonic changes between the first and second halves of both BP time series (300m & 500m) at the western

boundary. It seems that during the period 2014-2015 the semi-annual cycle was dominant and during the period 2016-2017 the annual cycle. This behavior can also be seen in figure 1. While this shift from one dominant time scale to the other is interesting, it is far beyond the scope of this study.

Explained variance [%]						
	300m WB (KPO 1134)			*500m WB (KPO 1135)*		
	AC	*SAC*	*A&SAC*	*AC*	*SAC*	*A&SAC*
2014-2015	*9,1*	*18,0*	*27,4*	*6,1*	*24,5*	*31,6*
2016-2017	*22,2*	*2,8*	*26,3*	*20,4*	*8,0*	*30,4*
full	*17,0*	*6,7*	*24,1*	*14,6*	*12,8*	*28,5*

235: Related question: Were the annual cycles from 4 years of data different from the annual cycles of 2-years of data on western boundary?

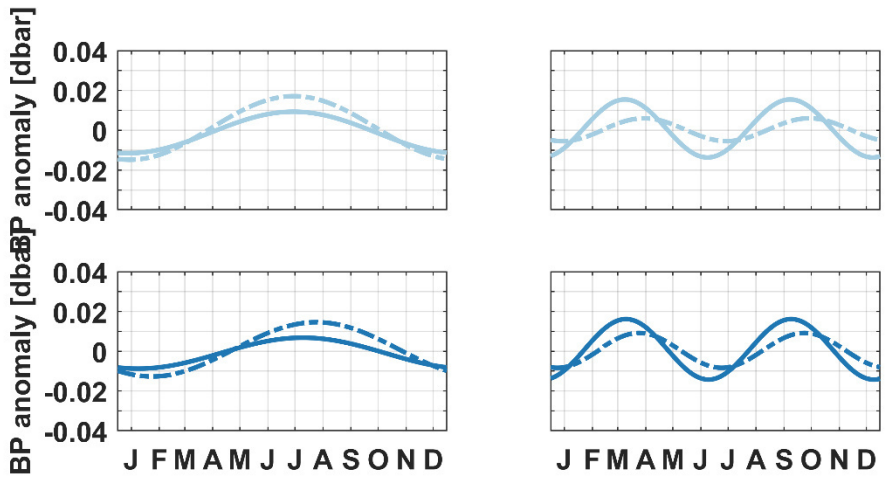

Figure 6 *Annual (left panels) and semi-annual (right panels) harmonics calculated for 2-year subsets - solid for 2014-2015 and dashed for 2016-2017 - of the available western boundary BP time series (similar to Fig. 5c,e in the manuscript) at 300m (upper panels) and 500m (lower panels).*

Shown in Fig.4 R2 are the annual and semi-annual harmonics calculated for 2-year subsets of the available western boundary BP time. Both, the annual and semi-annual harmonics show pronounced differences in their amplitudes (up to 50%) and minor differences in their phases (<1 month) between the two 2-year periods. Interestingly, the ratio of the amplitudes of the annual or semi-annual harmonic change between the two periods – please see the previous comment. However, the combined annual and semi-annual harmonics explain a similar fraction of the overall variance in both subsets of and in the full time series.

236-238: How would you estimate the uncertainty associated with only having seasonal cycle data on the eastern boundary after 11/2015? For example, if you swapped the seasonal cycle for eastern boundary time series data before 11/2015 what error do you make?

Within the fully equipped period 05/2014 - 11/2015 the correlation between the daily T'_G time series derived with 4 BPRs and the daily T'_G time series derived with WB BPRs and the EB combined annual

and semi-annual harmonics is high (R=0.85) and statistically significant. The latter can explain ~70% of the total variance in T'_G over fully equipped period. As this period is only 18 months, we assume the 30% of the variance that we seem to miss with our method to be related to the intra-seasonal signals we see in the spectra for EB BP (Fig.4 d,f).

236-238: You find that the eastern boundary is more important for seasonal cycle AMOC changes, which is consistent with previous studies, but how much confidence do you have in that result given you only have 2 years of data? Confidence can be derived from the analysis of INALT01 and SLA on the eastern boundary that is shown in the paper, but perhaps this is a point to articulate more strongly.

We added this sentence to the manuscript: "We derive confidence in our method from the comparison of the observed BP variations with variations in the simulated BP time series and in the SLA time series off Angola, both covering longer periods."

270: Figure 4 captioning and colors are a little confusing. Please label what is SSH, pressure 300 and 500 db.

We added this information to the y-axis labels in Fig.4 & 5.

274: How do your west coast and east coast bottom pressure findings compare with Meinen et al. (2018) where they also found energy on intraseasonal and interannual time scales in _1000 db bottom pressure data.

In contrast to the findings at 34.5°S, at 11°S, the BP time series at the eastern boundary exhibit more energy on intra-seasonal to seasonal time scales. Although, 90d and 120d peaks are found at 34.5°S as well as at 11°S, any comparison of intraseasonal variability between those two latitudes is difficult considering the differences in local wind regimes, impact or non-impact of equatorial forcing and eddy activity. Interannual variation of the SLA at the eastern boundary are, as discussed in the manuscript, thought to be related to equatorial dynamics and should not compare to findings at 34.5°S. We do also find hints for more energy on interannual timescales at the western boundary, but the time series are just not long enough for reliable estimates.

282: Are the corresponding western boundary percent variances similar in the first two years as the second two years? I know the eastern boundary has more of its variance explained by those harmonics, but this would give us some sense of the stationarity of those four years.

See our answer to some previous comments.

284: "Angola was" instead of "Angola as"

Corrected.

285: It is unclear why there are 3 phase lines in Figure 6b given that you only have annual and semi-annual harmonic. Please clarify.

*We show phase lines for the minimum of the annual harmonic in black and for the two minima of the semi-annual harmonic during a year in grey. The description was changed to "…*phases of the minima of the annual and semi-annual harmonics…*".*

292-293: If I'm not mistaken, you aren't showing the depth dependence of the western boundary phase information (i.e., Figure 6 is only for the eastern boundary) so you could say "not shown" or point to the Figure 5 left panels.

That's correct. As can be seen in Fig.5, amplitudes of the seasonal harmonics are small at the western boundary and phases very uncertain. As suggested, we added references to the corresponding panels in Figure 5 to the text.

294: You could mention here the similarities between the two 500-m deployments on the western boundary and how you get similar results. That builds more confidence in use of 2 years when you only have 2 years. (Similarly, you could break up 300-m western boundary record into two segments and compare first and second segment with full record)

We added a sentence to section 5.1: "This is also consistent between 2-year subsets of the western boundary BP time series."

297-298: Comment: It looks like the model bottom pressure seasonal cycle at 300m and 500m on the western boundary is almost non-existent, but on the eastern boundary the model captures the pressure seasonal cycle quite well.

Exactly. We rephrased this sentenced to "The model tends to overestimate the annual harmonic at the surface and generally underestimate seasonal variability in general at depth - especially at the western boundary the seasonal cycle of the simulated BP at 300 m and 500m depth is almost non-existent."

306: Here and elsewhere you should make clear if the +/-1.9 Sv is a standard deviation/ error/uncertainty.

Done.

307: If it is standard deviation suggest replacing "an Ekman transport of" with "a mean and standard deviation of Ekman transport of." or something like that.

Rephrased.

309: closing parentheses missing after (Fig. (7a,b)

Added, thanks.

314: In Figure 7c,d I would add years 2008 and 2009 on the left y-axis to help the reader easily follow which way time flows.

Done as suggested.

315: I'm confused about the sign of the wind stress. Westward wind anomaly should give you southward Ekman transport anomaly (strengthening) and you say the opposite. I think the sign of the winds is wrong, not the Ekman transport that you state. This is important to sort out.

You are right, the sign of the wind stress anomalies was wrong. Thanks for pointing this out. We corrected it.

316: Likewise, an eastward wind anomaly should give you a northward Ekman transport anomaly (weakening) and you say the opposite. I think the sign of the winds is wrong, not the Ekman transport that you state. This is important to sort out.

See previous comment.

328: You say/show that there is good agreement during the overlapping periods, but you don't give the correlation statistics. Are the correlations high and significant?

Within the period 05/2014-10/2015, when 5 BPRs were in place, we found high and statistically significant ($p<0.001$) correlations of 0.97 and 0.85 between the geostrophic transport time series estimated from the full set of 4 BPRs and estimated from 3 BPRs (WB 300m missing and replaced with combined annual & semi-annual harmonics) or 2 BPRs (EB 300m & 500m missing and replaced with combined annual & semi-annual harmonics), respectively.

347: "maximum northward transport in June" instead of "maximum in June"

Changed as suggested.

360: at the end of this sentence please indicate the appropriate figure panel to look at (i.e., Fig. 9e,f)

Done.

390: Suggestion "the NBUC (see Section 2.4)" so that readers are reminded how you compute NBUC.

It does not make sense to us to include the cross-reference to section 2.4 in this paragraph. We added it to the next paragraph: "Having a mooring array installed off the coast off Brazil measuring the Western Boundary Current system there (e.g. Hummels et al., 2015; see section 2.4), allows us to directly compare the seasonal variability of the NBUC in INALT01 with observations.".

415: It is hard to see the phase propagation in Figure 14b,c – perhaps add arrows or lines to better convey the sense of propagation.

Figures 14b,c were removed in the process of "streamlining" our manuscript.

419-420: Question: What is the depth of the mid Atlantic ridge in this region, is it deeper than 3000m?

Along 11°S, the top of the MAR is at about 2700m water depth. Actually, in the first submitted version of the manuscript it could be seen as a small white peak in figures 14 (b,c).

435-436: You may want to add something here like "but clearly a longer time series will help us in the future to refine these estimates" or something like that.

Added as suggested.

442: Unclear whether "They confirm" means "Kopte et al. (2018) confirmed" or that your findings in the manuscript confirm.

We changed the sentence to "Kopte et al. (2018) confirm….."

480: You could compare your results to more recent studies like Meinen et al. (2018) and Kersale et al. (2020) where they look at the seasonal cycle of the MOC at 34.5S from PIES moorings which may be relevant for your study.

Interestingly, the seasonal cycle of the geostrophic transport derive from PIES in Meinen et al. (2018) is very different to the estimate derived from ARGO/WOA presented in Dong et al. (2014). However, we deleted this discussion in order to streamline and shorten the manuscript. As we show in our study, seasonal variations in the geostrophic AMOC contribution at 11° S are driven by processes in the tropical Atlantic region. Therefore, a direct comparison between the Tropics and Subtropics on these timescales does not seem to be useful with regard to the mechanisms at work.

488: Here is one place where you can indicate if "long Rossby waves" here means "long, annual Rossby waves" (or if not annual, provide the period)

Changed to "annual".

525-526: You could indicate, that long-term PIES arrays have been deployed for a decade at 34.5S in the South Atlantic (Meinen et al. 2018; Kersale et al. 2020).

At SAMBA, the strategy to estimate the AMOC and its variability relies not only on BP measurement, but also on the acoustic travel times measured by the PIES on both sides of the basin (e.g. Meinen et al., 2017). The same approach was also used before to estimate the North Atlantic Current transport at 47° N (NOAC array; Roessler et al., 2015). This is different to our strategy mainly based on BP measurements. While at the WB we have PIES installed at 300m and 500m depth, the BP time series off Angola are measured with single BPRs.

Here, we wanted to make the point, that there is also a lot of potential in using only the BP measurements. However, it would be interesting to test how the travel times derived from the PIES installed off Brazil can add information to or reduce the uncertainty of our results. We added a sentence and hope to perform the respective analyses in the future.

Question: Some PIES moorings can be deployed with 4-year batteries and that makes it easier to determine pressure drift. Have you thought about doing so for future longterm deployments?

Thank you for the suggestion. We think, the best option would be to have more temporal overlapping observational periods of PIES, which however, requires more instruments. Nevertheless, we try to have the longest possible deployment periods.

References:

Frajka-Williams, E., I. J. Ansorge, J. Baehr, H. L. Bryden, M. P. Chidichimo, S. A. Cunningham, G. Danabasoglu, S. Dong, K. A. Donohue, S. Elipot, P. Heimbach, N. P. Holliday, R. Hummels, L. C. Jackson, J. Karstensen, M. Lankhorst, I. A. Le Bras, M. S. Lozier, E. L. McDonagh, C. S. Meinen, H. Mercier, B. I. Moat, R. C. Perez, C. G. Piecuch, M. Rhein, M. A. Srokosz, K. E. Trenberth, S. Bacon, G. Forget, G. Goni, D. Kieke, J. Koelling, T. Lamont, G. D. McCarthy, C. Mertens, U. Send, D. A. Smeed, S. Speich, M. van den Berg, D. Volkov, and C. Wilson, 2019: Atlantic Meridional Overturn- ing Circulation: Observed transport and variability, Frontiers in Marine Science, 6:260, doi: 10.3389/fmars.2019.00260.

Kersalé, M., C. S. Meinen, R. C. Perez, M. Le Henaff, D. Valla, T. Lamont O. T. Sato, S. Dong, T. Terre, M. van Caspel, M. P. Chidichimo, M. van den Berg, S. Speich, A. R. Piola, E. J. D. Campos, I. Ansorge, D. L. Volkov, R. Lumpkin, and S. Garzoli, 2020: Highly Variable Upper and Abyssal Overturning Cells in the South Atlantic, Science Advances, 6, eaba7573, 10.1126/sciadv.aba7573.

Imbol Koungue, R. A., S. Illig, and M. Rouault, 2017: Role of interannual Kelvin wave propagations in the equatorial Atlantic on the Angola Benguela Current system. J. Geophys. Res. Oceans, 122, 4685–4703, https://doi.org/10.1002/2016JC012463.

Meinen, C. S., S. Speich, A. R. Piola, I. Ansorge, E. D. Campos, M. Kersale, T. Terre, M. P. Chidichimo, T. Lamont, O. T. Sato, R. C. Perez, D. Valla, M. Le Henaff, S. Dong, and S. L. Garzoli, 2018: Meridional Overturning Circulation transport variability at 34.5S during 2009-2017: Baroclinic and barotropic flows and the dueling influence of the boundaries, Geophysical Research Letters, 45, 4180-4188, doi: 10.1029/2018GL077408.

Dong, S., Baringer, M. O., Goni, G. J., Meinen, C. S., and Garzoli, S. L.: Seasonal variations in the South Atlantic Meridional Overturning Circulation from observations and numerical models, Geophys. Res. Lett., 41, 4611– 4618, doi:10.1002/2014GL060428, 2014.

Hummels, R., Brandt, P., Dengler, M., Fischer, J., Araujo, M., Veleda, D., and Durgadoo, J. V.: Interannual to decadal changes in the western boundary circulation in the Atlantic at 11° S, Geophys. Res. Lett., 42, doi:10.1002/2015GL065254, 2015.

Kanzow, T., Cunningham, S. A., Johns, W. E., Hirschi, J. J., Marotzke, J., Baringer, M. O., Meinen, C. S., Chidichimo, M. P., Atkinson, C., Beal, L. M., Bryden, H. L., and Collins, J.: Seasonal Variability of the Atlantic Meridional Overturning Circulation at 26.5° N. J. Climate, 23, 5678–5698, doi:10.1175/2010JCLI3389, 2010.

Meinen, C. S., Garzoli, S. L., Perez, R. C., Campos, E., Piola, A. R., Chidichimo, M.-P., Dong, S., and Sato, O. T.: Characteristics and causes of Deep Western Boundary Current transport variability at 34.5° S during 2009-2014, Ocean Sci., 175-194, doi:10.5194/os-13-175-2017, 2017.

Lumpkin, R., and K. Speer, 2003: Large-Scale Vertical and Horizontal Circulation in the North Atlantic Ocean. J. Phys. Oceanogr., 33, 1902–1920, https://doi.org/10.1175/1520-0485(2003)033<1902:LVAHCI>2.0.CO;2.

Roessler, A., Rhein, M., Kieke, D., and Mertens, C.: Long-term observations of North Atlantic Current transport at the gateway between western and eastern Atlantic. J. Geophys. Res.-Oceans, 120,4003–4027. doi:10.1002/2014JC010662, 2015.

Schott, F. A., Dengler, M., Zantopp, R., Stramma, L., Fischer, J., and Brandt, P.: The Shallow and Deep Western Boundary Circulation of the South Atlantic at 5° –11° S. J. Phys. Oceanogr., doi:10.1175/JPO2813.1, 2005.

Seasonal variability of the Atlantic Meridional Overturning Circulation at 11°S inferred from bottom pressure measurements

Josefine Herrford[1], Peter Brandt[1,2], Torsten Kanzow[3], Rebecca Hummels[1], Moacyr Araujo[4], Jonathan V. Durgadoo[1,2]

[1]GEOMAR Helmholtz Centre for Ocean Research, Kiel, Germany
[2]Christian-Albrechts-Universität zu Kiel, Kiel, Germany
[3]Alfred Wegener Institute, Bremerhaven, Germany
[4]Department of Oceanography Federal University of Pernambuco, Recife, Brazil

Correspondence to: Josefine Herrford (jherrford@geomar.de)

Abstract. Bottom pressure observations on both sides of the Atlantic basin, combined with satellite measurements of sea level anomalies and wind stress data, are utilized to estimate variations of the Atlantic Meridional Overturning Circulation (AMOC) at 11° S. Over the period 2013-2018, the AMOC and its components are dominated by seasonal variability, with peak-to-peak amplitudes of 12 Sv for the upper-ocean geostrophic transport, 7 Sv for the Ekman and 14 Sv for the AMOC transport. ~~The observed seasonal cycles of the AMOC, its components as well as the Western Boundary Current as observed with current meter moorings are in general good agreement with results of an ocean general circulation model.~~ The characteristics of the observed seasonal cycles of the AMOC and its components are compared to results from an ocean general circulation model, which is known to reproduce the variability of the Western Boundary Current on longer timescales. The observed seasonal variability of zonally integrated geostrophic velocity in the upper 300 m is controlled by pressure variations at the eastern boundary, while at 500 m depth contributions from the western and eastern boundaries are similar. The model tends to underestimate the seasonal pressure variability at 300 and 500 m depth, ~~slightly stronger~~especially at the western boundary, which translates into the upper-ocean geostrophic transport. ~~–~~ In the model, seasonal AMOC variability at 11° S is governed, besides the Ekman transport, by the geostrophic transport variability in the eastern basin. ~~Here, long Rossby waves originating from equatorial forcing are known to be radiated from the Angolan continental slope and propagate westward into the basin interior.~~ The geostrophic contribution of the western basin to the seasonal cycle of the AMOC ~~to AMOC seasonal variability~~ is instead comparably weak as transport variability in the western basin interior related to local wind curl forcing ~~due to locally forced Rossby waves~~ is mainly compensated by the Western Boundary Current. Our analyses indicate, that while some of the uncertainties of our estimates result from the technical aspects of the observational strategy or processes being not properly represented in the model, uncertainties in the wind forcing are particularly relevant for AMOC estimates at 11° S.

1 Introduction

The Atlantic Meridional Overturning Circulation (AMOC) plays a major role in the global oceanic heat budget. About 88% ~~O~~of the maximum heat transport in the subtropical North Atlantic ~~of 1.3 PW found in the subtropical North Atlantic~~ (1.3 PW; e.g. Lavin et al., 1998) ~~about 88%~~ are carried by the AMOC (Johns et al., 2011). Because of the AMOC, there is substantial northward heat transport across the Atlantic equator (e.g. Talley, 2003), which is unique among global oceans. Simplifying the circulation in the Atlantic to a two-dimensional latitude-depth plane, the AMOC connects warm waters flowing northward in the upper ocean and cold waters flowing southward at depth across all latitudes ~~by~~ through ~~downward and upward motion~~water mass transformation, for example, in the subpolar North Atlantic or near the Southern Ocean (e.g. Buckley & Marshall, 2016). With the AMOC representing the strongest mode of northward heat transport ~~accomplished~~ by the ocean, it is essential to provide the observational evidence of the mechanisms that control its structure and variability in order to understand the present-day climate, validate climate simulations and improve predictions. ~~providing the observational evidence of the mechanisms that control its structure and variability is therefore of high priority for understanding the present day climate, validating climate simulations and improving predictions.~~

Historically, the strength and structure of the AMOC was estimated based on shipboard hydrographic sections ~~, which focused on~~ establishing the mean AMOC strength and related heat transport (e.g. Richardson, 2008). The first trans-basin mooring array - the RAPID/MOCHA transport array at 26° N - continuously measures~~ing~~ the temporal variability of the AMOC ~~was set up in~~since the early 2000s (Hirschi et al., 2003). ~~From the observations at 26° N, we learned~~Those observations showed~~,~~ that large AMOC variations can occur on a range of timescales - from weeks to decades (e.g. Srokosz & Bryden, 2015). Kanzow et al. (2007) showed, that not only the Ekman, but even more the geostrophic contribution to the AMOC, exhibit pronounced high-frequency variability with periods up to few weeks. Kanzow et al. (2010) demonstrated that the strong seasonal cycle in the AMOC strength at 26° N leads to aliasing, when estimating the AMOC strength from single hydrographic sections. ~~With the identification of a strong seasonal cycle in the AMOC strength at 26° N, Kanzow et al. (2010) demonstrated that AMOC estimates inferred from single hydrographic sections are subject to aliasing.~~ They also found the upper-ocean geostrophic AMOC contribution to dominate on seasonal time scales, while Chidichimo et al. (2010) discovered those to be primarily driven by processes at the eastern boundary.

Today, there are several ongoing international efforts monitoring the AMOC at selected latitudes (e.g. Frajka-Williams et al., 2019), such as - the OSNAP array in the subpolar North Atlantic (since 2014; Lozier et al., 2019), the RAPID array in the subtropical North Atlantic at 26° N (since 2004; Cunningham et al., 2007; McCarthy et al., 2015), the MOVE array in the tropical North Atlantic at 16° N (since 2001; Kanzow et al., 2008; Send et al., 2011; Frajka-Williams et al., 2018), the SAMBA array in the subtropical South Atlantic at 34.5° S (since 2009; Meinen et al., 2018) – as well as other programs measuring important components of the overturning, such as - the Western Boundary Current (WBC) arrays at 53° N (since 1997; Zantopp et al. 2017) ~~and,~~ at 39° N (Line W; 2004-2014; Toole et al., 2017) and at 11°S (2000-2004 and since 2013; Hummels et al., 2015), the array across the North Atlantic Current at 47° N (NOAC array; Roessler et al., 2015), the deep overflow observations

through Denmark Strait (Jochumsen et al., 2017) or Faroe Bank Channel (Hansen et al., 2016). In this study, we will present the first estimate of basin-wide AMOC variations in the tropical South Atlantic - from the TRACOS (Tropical Atlantic Circulation and Overturning at 11° S) array.

The western tropical South Atlantic constitutes a key region for the exchange of water masses, heat and salt between the Southern and Northern Hemispheres (Biastoch et al., 2008a; Schmidtko & Johnson, 2012; Kolodziejczyk et al.,2014; Hummels et al.,2015; Lübbecke et al., 2015; Herrford et al., 2017). Several observational and modelling studies (e.g. Rühs et al., 2016; Zhang et al., 2011) suggest that 11° S is a good place to monitor water mass signal propagation, changes in the WBC transports and, with that, changes in the AMOC transport. At 11° S the WBC regime is comprised of the northward North Brazil Undercurrent (NBUC) with a subsurface velocity maximum at about 200 m and the southward Deep Western Boundary Current (DWBC) below 1200 m (e.g. Schott et al., 2005). The NBUC is known to originate from the southern branch of the South Equatorial Current (da Silveira et al., 1994), which transports subtropical waters towards Brazil and bifurcates between 14-28° S (Stramma and England 1999; Boebel et al. 1999; Wienders et al., 2000). ~~Wind-driven variability in the South Atlantic subtropical gyre, and therefore, variations in the bifurcation latitude are thought to influence the strength of the NBUC farther downstream on different time scales (e.g. Rodrigues et al., 2007; Silva et al., 2009).~~ From 2000 to 2004, a first mooring array was deployed at 11° S to observe the variability of the WBC and its components –the NBUC and the DWBC below. Schott et al. (2005) found the NBUC to carry 25 Sv northward on average. The NBUC ~~shows~~ showed a strong seasonal cycle, which seems to be out of phase with the seasonal variations in the DWBC. Intraseasonal signals could also be observed: Dengler et al. (2004) described a spectral peak in the velocity time series at a period of 60-70 days, which ~~could be~~was observed in most of the moored records, but was strongest within the DWBC. They concluded that the DWBC transport at 11° S is mainly accomplished by migrating eddies. Further, Veleda et al. (2012) could relate variability at periods of 2-3 weeks to coastal trapped waves (CTWs) propagating from 22-36° S equatorward along the Brazilian coast. In July 2013, a similar mooring array was again deployed at 11° S (Hummels et al., 2015), and is still in place. Comparing the two observational periods, Hummels et al. (2015) did not find significant changes in the averaged NBUC and DWBC transports. Furthermore, they could show that the interannual NBUC variability observed between 2000-2004 is consistent with the output of a forced ocean general circulation model (OGCM) named INALT01. Decadal variability in INALT01 ~~, however,~~ was also found to be similar to transport estimates based on historical hydrographic observations from Zhang et al. (2011). To date, Zhang et al. (2011) provide the only NBUC time series derived from hydrographic observations spanning several decades. They estimated multi-decadal variability of the NBUC to be of similar order as its seasonal cycle and, because of the connection to the Atlantic Multidecadal Variability, suggested the NBUC to serve as an index for AMOC variations on these time scales. In a model study, Rühs et al. (2016) found decadal to multi-decadal buoyancy-forced changes in the AMOC transport to manifest themselves in NBUC transport (at 6° S), however these changes are also ~~but also to be~~ masked by interannual wind-driven variability.

With the resumption of the mooring array at 11° S in 2013, the observational program was also extended by installing a mooring array for direct velocity measurements across the continental slope off Angola. Studies based on these observations

showed that the circulation there is weak and dominated by seasonal variability associated with remotely forced waves (Kopte et al., 2017; 2018). As shown in several model studies, most of the intraseasonal (T>120 days) to interannual variability in that region is induced by a wave response to equatorial wind forcing that generates equatorial Kelvin waves propagating eastward and, while reaching the eastern boundary, transferring a part of their energy as CTWs further to the south towards 11° S (Illig et al., 2004; Illig et al., 2018; Bachèlery et al., 2016; Imbol Koungue et al., 2017).

Besides the moored observations at 11° S, PIES (Pressure Inverted Echo Sounders) or single bottom pressure recorders (BPRs) were deployed on both sides of the Atlantic. Within some of the other programs targeting AMOC fluctuations, – such as RAPID (Kanzow et al. 2010~~, McCarthy et al., 2015~~, Meinen et al. 2013, McCarthy et al., 2015), MOVE (Kanzow et al., 2006, 2008) and SAMBA (Meinen et al., ~~2017,~~ 2018; Kersale et al., 2020) – bottom pressure (BP) measurements ~~are part of the "moored end point method", combining a~~are used to estimate the time-varying portion of a barotropic reference velocity ~~time-varying reference velocity estimated from zonal BP differences~~ which is then combined with the internal geostrophic velocity derived from differences in dynamic height derived from full-depth dynamic height moorings or the PIES travel times. But, circulation changes in z-coordinates can also be estimated using only a series of bottom pressure measurements installed at different depths on the western and eastern continental slopes. ~~Circulation changes in z-coordinates can even more straightforward be estimated by measuring the pressure differences between the eastern and western boundary at each depth~~. In a model study, Bingham and Hughes (2008) showed that this works well down to around 3000 m, even with only western boundary measurements. In our study, we use the BP differences across the basin at 300 m and 500 m depth to estimate the geostrophic contribution to AMOC variations in the tropical South Atlantic over the period 2013-2018 and investigate its seasonal variability ~~in more detail~~.

2 Observational Data

~~1~~2.1 Bottom pressure time series

Over the period 2013-2018 five BPRs were deployed at 11° S (Table 1). In ~~July~~ May 2013, together with the WBC mooring array, two bottom-mounted PIES were installed across the Brazilian continental slope at 300 m and 500 m depth. PIES measure the acoustic travel time to the surface, as well as bottom pressure. In this study, we only used the BP time series. One year later another set of PIES was deployed at the same locations. While of the first set only the 500 m sensor could be recovered, the second set was maintained in September 2016 and spring 2018. Note, that the two PIES, KPO 1109 and KPO 1135 (Table 1) were located only ~1 km away from each other over the period 05/2014 – 10/2015. At the eastern boundary off Angola, two SBE 26plus sensors (single or attached to an ADCP shield) measured pressure at 300 m and 500 m depth from 07/2013 to 11/2015. The instruments were re-deployed, but could not be recovered again. We assume, that they were lost due to extensive fishing in the region.

For our analyses, the available BP records ~~are~~ were de-spiked, interpolated from an original sampling rate of 10 minutes to hourly values and de-tided using harmonic fits with tidal periods shorter than 35 days. All tidal harmonics ~~are~~ were calculated

performing a classical harmonic analysis ~~using the "Unified Tidal analysis and prediction" MATLAB® software (UTide;~~ Codiga, 2011). The tidal models for T < 35 days capture between 97.0-99.6% of the total variance in the original BP time series. After removing these higher-frequency tides, the remaining variance is mainly related to seasonal variations and low-frequency instrument drifts. Instrument drifts vary substantially between the five instruments: While KPO 1106 shows almost no drift, all other sensors exhibit a combination of exponential and linear behaviour, but with different signs and at different rates (Fig. ~~2~~1(a)). Unfortunately, we ~~are~~ were not able to directly relate individual drift behaviour to pressure effects or material creep. Earlier studies (e.g. Watts & Kontoyiannis, 1990; Johns et al., 2005; Kanzow et al., 2006; Cunningham et al, 2009) found subtracting a least-squares exponential-linear fit of the form $P_{Drift}(t) = a[1 - e^{-bt}] + ct + d$ from the pressure time series to be the procedure that works best for the PIES. As the SBE26plus recorders were also equipped with Quartz pressure sensors, we decided to "de-drift" all five sensors similarly by subtracting exponential-linear fits as described above. Kanzow et al. (2006) also discussed the problem of this empirical de-drifting not being able to distinguish between the instrumental drift and ocean signals of the order of or longer than the time series. This means that, for example, seasonal signals can leak into the fit and its removal from the time series can reduce seasonal signals in return. We attempted to solve this problem by iteratively fitting an exponential-linear drift as well as annual and semi-annual harmonics. ~~We started with a~~The first guess of the exponential-linear drift~~,~~ was removed ~~it~~ from the original time series and ~~fitted~~ annual and semi-annual harmonics were fitted to the de-drifted time series. ~~The~~ This first guess was iteratively improved ~~in each iterative step~~ by calculating new exponential-linear fits after subtracting the iteratively improved annual and semi-annual harmonics from the original data. After three repetitions the ~~resulting~~ fits tended to converge. Both fits from the third repetition are shown in Fig. ~~2~~1(a). For further analyses, we removed the derived instrument drift from the original BP time series and averaged to daily values (Fig. ~~2~~1(b)).

~~1~~2.2 Sea level anomalies

To estimate pressure variability at the surface, we used sea level anomalies (SLA) from the delayed-time ''all-sat-merged'' data set of global sea surface height, produced by Ssalto/Duacs and provided by the Copernicus Marine Environment Monitoring Service (CMEMS). The multi-satellite altimeter sea surface heights are mapped on a 0.25° x 0.25° grid (e.g. Pujol et al., 2016) and are available for the period 1993-2018 at daily resolution. To obtain pressure variation near the boundaries, SLA grid points ~~are~~ were chosen closest to the Brazilian and Angolan coasts at 11° S, respectively. ~~We tested~~ T~~t~~he sensitivity of our results to SLA changes with distance to the coast (Fig. 2(c,d)) was tested: At the western boundary, off Brazil, the phase of the annual harmonic slightly changes with distance to the coast – about 30 days over 0.5° longitude. At the eastern boundary, off Angola, ~~we found~~ the phases of both annual and semi-annual harmonics ~~to be~~are constant over the distance between the location of the 300 m BPR and the coast.

~~1~~2.3 Wind stress

In order to estimate the Ekman contribution to AMOC variability at 11° S we used gridded daily wind stress fields from Metop/ASCAT scatterometer retrievals. Those are available for the period 2007-2018 and with a spatial resolution of 0.25° x 0.25° (Bentamy & Croizé-Fillon, 2012). The near-surface Ekman transport ~~is~~ was estimated as the zonal integral of the zonal wind stress component between 10.5-11° S (see Eq. (7) in section 4.1).

~~1~~2.4 NBUC transport time series

To estimate the western boundary current transport, we computed ~~We show~~ a transport time series of the NBUC (Fig.13a), which is derived from four current meter moorings spanning the width of the NBUC at 11° S~~.~~ and represents an update from previous studies (Schott et al., 2005; Hummels et al., 2015). Record gaps were filled with empirical orthogonal functions (EOFs) derived from the mooring data. Moored time series were finally mapped into sections every 2.5 days using a Gaussian-weighted interpolation with horizontal mapping scales of 20 km with a cutoff radius of 150 km and vertical mapping scales of 60 m with a cutoff radius of 1500 m. The NBUC transport was computed by integrating the total flow (including northward and southward flow) within a predefined box (see Hummels et al. (2015) for further details). ~~The NBUC transport is calculated integrating the total flow (including northward and southward flow) within a predefined box bounded vertically by the surface and the neutral density surface γn =27.7 kg m-3, and horizontally by the Brazilian coast and the longitude 34.5° W. These transports represent updates from previous studies (Schott et al., 2005; Hummels et al., 2015).~~

3 Model Data

To validate the observational strategy, we used the 5-daily output from a hindcast experiment with the global ocean/sea-ice Ocean General Circulation Model configuration `INALT01`. It is based on the NEMO (Nucleus for European Modelling of the Ocean v3.1.1; Madec, 2008) code and developed within the DRAKKAR framework (The DRAKKAR Group, 2014). INALT01 is a global 1/2° configuration with a 1/10° refinement between 70°W-70°E and 50°S-8°N, improving the representation of the western boundary current regime in the South Atlantic and extended Agulhas region (Durgadoo et al., 2013). It uses a tripolar horizontal grid, 46 vertical levels with increasing grid spacing and is forced by interannually varying air-sea fluxes (1948-2007) from the CORE2b data set (Coordinated Ocean-ice Reference Experiments; Large & Yeager, 2009). Sea surface elevation and wind stress are then prognostic variables: INALT01 uses the filtered free surface formulation for the surface pressure gradient and ~~SSH is then a prognostic variable.~~calculates surface wind stress from relative winds using the CORE2b bulk formulae.~~-~~ This particular model configuration has been previously used in the region. South of Africa it was used for validating a method of determining Agulhas leakage from satellite altimetry (Le Bars et al., 2014). In the WBC region Hummels et al. (2015) found interannual NBUC variability derived from moored observations and decadal NBUC variability from geostrophic estimates (Zhang et al., 2011) to be consistent with the INALT01 output. Further, the simulated overturning streamfunction (in neutral density classes) at 11°S is in good agreement with the vertical structure and amplitude of an estimate

based on shipboard observations conducted in 1994 (Lumpkin & Speer, 2003). Our analysis employs 2-dimensional (longitude-depth) sections of temperature, salinity and velocity, as well as surface elevation and wind stress fields along 11° S for the simulated period 1978-2007. Surface wind stress fields are additionally shown for the years 2008-2009.

4 Methods

4.1 Computation of AMOC transport variations from BP observations

The structure of the AMOC is often described using the overturning transport stream function $\psi(y,z,t)$, which is derived from integrating the meridional velocity component, v, zonally (from the ~~eastern~~ western (x_{WEB}) to the ~~western~~ eastern boundary (x_{EWB})) and ~~accumulating it~~ vertically:

$$\psi(y,z,t) = \int_{z}^{0} \int_{x_{WB}}^{x_{EB}} v(x,y,z',t)\,dx\,dz' \quad (1)$$

with x being longitude, y latitude, z the vertical coordinate pointing upward and t time. This reduces a complex three-dimensional circulation system to a two-dimensional one. The AMOC strength or transport is commonly defined as the maximum of ψ over depth and typically expressed in Sverdrups [1 Sv = 10^6 m^3 s^{-1}]. At any chosen latitude, Ψ_{MAX} can be decomposed into Ekman and geostrophic components (thereby generally neglecting small ageostrophic, non-Ekman components):

$$\psi_{MAX}(y,t) = T_{AMOC}(y,t) \approx T_G(y,t) + T_{EK}(y,t) \quad (2)$$

Variations in the basin-wide upper-ocean meridional geostrophic transport T_G at a certain latitude can be derived from the differences between the bottom pressure at the eastern (P_{EB}) and western (P_{WB}) basin boundaries. At 11° S, we use bottom pressure measurements on both sides of the basin at 300 m and 500 m depth. Figure 3 displays the observational strategy.

Our ~~Unfortunately, technology limits our~~ method is limited by the fact that ~~as it is not possible to determine precisely~~ the depth levels ~~at which~~ of the instruments ~~were placed~~ with respect to equi-geopotential surfaces are not known and, thus, only velocity anomalies can be determined (e.g. Donohue et al., 2010). However, the differences between eastern and western boundary pressure anomalies from BPRs have successfully been used to estimate temporal fluctuations of the geostrophic contribution to AMOC variability (e.g. Kanzow et al., 2007).

At ~~those depths, which are equipped with~~ the BPRs depths, anomalies of the geostrophic transport per unit depth $V'_G(z,t)$ ~~are~~ were calculated as ~~follows~~:

$$V'_G(z,t) = \frac{1}{\rho_0 \cdot f} \cdot \left(P'_{EB}(z,t) - P'_{WB}(z,t)\right) \quad (3)$$

P'_{EB} and P'_{WB} are the pressure anomalies at the eastern and western boundary with respect to the time mean, respectively, f the Coriolis parameter and ρ_0 a mean sea water density. At the surface, $V'_G(z = 0, t)$ can be calculated accordingly from sea level anomalies, η'~~, at the eastern and western boundary~~:

$$V'_G(z = 0, t) = \frac{g}{f} \cdot (\eta'_{EB}(t) - \eta'_{WB}(t)) \quad (4)$$

with g being the acceleration of gravity. Additionally, a level of no motion is prescribed ~~to be~~ at 1130 m, such that $V'_G(z = -1130\ m, t) = 0$ at all times. This 'level of no motion' is ~~estimated~~ based on the velocity field from the INALT01 model configuration and defined as the ~~depth of the~~ local zero-crossing depth of v, averaged across the basin and over time. The maximum of the corresponding stream function ~~is~~ averaged over time is located at z = -1072 m. Earlier studies in this region, ~~presenting transport estimates for 11° S,~~ used a level-of-no-motion at the depths of $\sigma_1 = 32.15$ kg m^{-3} (at about 1150 m; e.g. Stramma et al., 1995; Schott et al., 2005). The sensitivity to the choice of the level of no motion was tested between 800-1300 m and the obtained AMOC transport changed by less than 10%.

We use two different methods to approximate the vertical structure of V'_G:

1. Piecewise linear interpolation of V'_G between the 4 data points at 0 m, 300 m, 500 m and 1130 m depth – denoted as $V'_{G\ Points}$ or $T'_{G\ Points}$ throughout the study.
2. Regression of the 1st and 2nd EOFs, i.e. the two dominant vertical structure functions of the geostrophic transport per unit depth derived from density and sea level anomalies in INALT01, $V'_{G\ SIM\ P(z)}$ (see chapter 4b), onto the 3 data points at 0 m, 300 m and 500 m depth thereby relaxing the no-flow condition at 1130 m depth. The first (second) dominant vertical structure function explains 90.3% (9.6%) of the variance contained in $V'_{G\ SIM\ P(z)}$ ~~and the second 9.6%.~~ The resulting transport variations ~~resulting from this method~~ are denoted as $V'_{G\ EOFs}$ or $T'_{G\ EOFs}$ ~~in the following~~.

Upper-ocean geostrophic transport variations, T'_G, ~~are~~ were then calculated by vertically integrating the approximated V'_G profile from z_3=-1130 m up to the surface. ~~Using the first method, z_3 is defined as the 'level of no motion' in the simulated mean velocity field, separating the northward flow of warm Central Waters and Antarctic Intermediate Waters from the southward flow of deep waters below. For the second method, z_3 does not represent a 'level of no motion'.~~

$$T'_G(t) = \int_{z_3}^{0} V'_G(z, t)\ dz \quad (5)$$

Using the first method, z_3 is defined as the 'level of no motion' ($V'_G(z_3) = 0$), whereas for the second method $V'_G(z_3)$ might vary with time.

Finally, AMOC transport variations (T'_{AMOC}) can be derived by adding local Ekman transport anomalies T'_{EK}.

$$T'_{AMOC}(t) = T'_G(t) + T'_{EK}(t) \quad (6)$$

~~Those~~ The latter can efficiently be estimated from the zonal component of the wind stress, τ_x, at 11° S according to

$$T_{EK}(t) = -\int_{x_{WB}}^{x_{EB}} \frac{\tau_x(x,t)}{\rho_0 \cdot f} dx \quad (7)$$

and subtracting the temporal average.

In the following, all mean transports are presented together with the standard error $SE = \sigma/\sqrt{N/n_d}$, where σ is the standard deviation and n_d the decorrelation time scale of the respective time series of length N.

~~The a~~Annual and semi-annual harmonics for all pressure time series (section 5.1) are presented together with uncertainties for their amplitudes, which were ~~determined using the UTide software (Codiga, 2011) and are presented together with an uncertainty estimate for their amplitudes in section 5a. The uncertainties for the amplitudes of the combined annual and semi-annual harmonics are~~ derived by ~~, first,~~ low-pass filtering the pressure time series with a cutoff of 170 days~~,~~ and ~~then~~ subsequently calculating the 95th percentile ~~around~~ of the deviations from the derived annual and semi-annual harmonics for every day of the year.

Following the observational strategy (Fig. 3), ~~we would need~~BPRs at least at four different locations ~~at (~~two depth levels~~) to be equipped with BPRs in order~~ are required to derive basin-wide geostrophic transport variations in the upper 1130 m of the water column. While ~~we had~~ five recorders were in place over the period ~~15/~~05/2014-~~02/~~10/2015, ~~there are~~ no BP measurements at 300 m depth off Brazil are available before 05/2014 and none at all off Angola since 11/2015. In this study, we ~~find~~ found seasonal variability to dominate all ~~of the~~ pressure time series at 11° S (see section 5.1). The combined annual and semi-annual cycles explain 44-61 % of the variance in the daily BP time series at the eastern boundary and 18-24 % of the variance at the western boundary. Therefore, we decided to "replace" the missing sensors with the combined annual and semi-annual harmonics derived from the available BP time series. This means, for example, that the geostrophic transport after 11/2015 is derived from the differences between measured BP variations at the western boundary and repeated annual and semi-annual harmonics – as derived from earlier years – at the eastern boundary. We derive confidence in our method from the comparison of the observed BP variations with variations in the simulated BP time series and in the SLA time series off Angola, both covering longer periods.

4.2 Using the OGCM INALT01 as a 'testing area'

~~In order to~~To validate our strategy for the computation of AMOC variations from the BP observations and to better ~~, but also to~~ understand the observed seasonal variability, we simultaneously ~~analyze~~ analyzed the output of the OGCM INALT01 (see section 3).

In INALT01 we can diagnose AMOC variations, $T'_{AMOC\ SIM}$, ~~directly~~ from the velocity field using Eq. (1) and Eq. (2), i.e. by directly integrating the simulated meridional velocity component at 11° S horizontally across the basin and vertically from 1130 m to the surface. The zonally integrated Ekman transport $T_{EK\ CORE2bSIM}$ at 11° S is derived with Eq. (7) from ~~CORE2b~~

INALT01 wind stress~~, which is used to force INALT01~~. According to Eq. (6) the simulated upper-ocean geostrophic transport anomaly $T'_{G\ SIM}$ is then ~~the difference between~~ $T'_{AMOC\ SIM} - T'_{EK\ SIM}$ ~~and $T'_{EK\ CORE2b}$~~.

Alternatively, we can ~~also~~ derive ~~an estimate of the simulated upper ocean geostrophic transport anomaly,~~ $T'_{G\ SIM\ P(z)}$ according to our observational strategy based on ~~by calculating~~ BP fields ~~at 11° S~~ from the modelled hydrographic fields and sea level. The model pressure field is given by

$$p(x,z,t) = g \cdot \int_{z}^{0} \rho(x,z',t)dz' + g \cdot \rho_0 \cdot \eta(x,t) \quad (8)$$

with g being the acceleration of gravity, ρ the seawater density as function of z and η the sea level. Taking the BP along the continental slopes (at each depth level) of Brazil and Angola from Eq. (8), the simulated upper ocean geostrophic transport anomalies, $V'_{G\ SIM\ P(z)}$ and $T'_{G\ SIM\ P(z)}$, can be derived from the pressure differences across the basin using Eq. (3) and Eq. (5). Under the assumption, that ageostrophic non-Ekman velocities are negligible, $T'_{G\ SIM}$ and $T'_{G\ SIM\ P(z)}$ should agree and particularly should show the same seasonal cycles. ~~We also test or observational strategy by applying~~Additionally, we test the two methods used to approximate the vertical structure of V'_G from the observations (see section 4.1): 1. Piecewise linear interpolation between values of $V'_{G\ SIM\ P(z)}$ at 0 m, 300 m, 500 m depth and a level of no motion at 1130 m depth –denoted as $V'_{G\ SIM\ Points}$ or $T'_{G\ SIM\ Points}$ in the following, and~~.~~ 2. Regression of the 1st and 2nd EOFs of $V'_{G\ SIM\ P(z)}$ onto the values $V'_{G\ SIM\ P(z)}$ at 0 m, 300 m, 500 m depth – deriving $V'_{G\ SIM\ EOFs}$ or $T'_{G\ SIM\ EOFs}$. These different transport estimates from INALT01 ~~are~~ were used to validate the methods applied to the observations (see section 5.3). ~~As the resulting uncertainties are discussed mainly with regard to variations of the seasonal cycle, the method test (particularly including the test of uncertainties due to the coarse vertical sampling at only few locations, i.e., at 300 m and 500 m depth) is part of section 5.3 presenting the seasonal variability of AMOC components.~~ In section 5.4, we use INALT01 to identify relevant mechanisms of the seasonal AMOC variability at 11° S, including specifically a comparison of the seasonal variability of the NBUC transport derived from observations and INALT01. For the sake of simplicity, in INALT01, unlike for the calculations from observations, the NBUC transport ~~is~~ was calculated above a fixed depth of 1130 m and west of 34.55° W.

5 Results

5.1 Ocean pressure variability at 11°S

All of the ocean pressure time series ~~we present~~ in this study, i.e. at the surface from SLA (Fig. 2 ~~(~~a and~~,~~ b~~)~~), at 300 m and 500 m depth from the BPRs (Fig. 1~~(~~ b~~)~~), at the western or eastern boundary, are dominated by seasonal variability. The corresponding periodograms ~~are shown as colored curves in Fig. 4 and~~ all exhibit pronounced peaks at periods of the annual and semi-annual cycles (colored curves in Fig.4).

~~Although we will mainly focus~~ The main focus here is on seasonal variability ~~in the following~~, however there are~~it is worth to mention~~ some other interesting peaks in the periodograms indicating ~~: There is~~ energy on intraseasonal and interannual time scales. Off Brazil, variability at a period of 70 days (Fig. 4 c and d) is very likely related to the DWBC eddies described by Dengler et al. (2004), which are thought to dominate the DWBC flow at 11° S and ~~can~~ influence the upper water column as well (e.g. Schott et al., 2005). The periodograms of SLA at the eastern boundary (Fig. 4 b) exhibit peaks at 90 days, 120 days and 2 years. Variability at periods of 90 days and 120 days were also observed by Kopte et al. (2018) in velocity time series from moored observations off Angola and are likely associated with the passage of CTWs. Based on numerical experiments, Bachèlery et al. (2016) showed that SLA variability along the African coast is on intraseasonal time scales (T<105 days) primarily driven by local atmospheric forcing, while at periods >120 days it can mostly be explained by equatorial forcing. Further, Polo et al. (2008) suggested that part of the intraseasonal variability is related to year-to-year variations of the seasonal cycle. Interestingly, the OGCM INALT01 does reproduce the spectral peaks at 2 years, 120 days and 90 days in the SLA off Angola, but not the 70 days period observed in any of the BP time series.

We ~~find~~ found the relative importance of seasonal variability to be most pronounced near the surface off Angola in both, the observations and the model (Fig. 4). The combined annual and semi-annual harmonics of the observed pressure time series explain most of the variance there – 61% at the surface, 58% at 300 m depth, 44% at 500 m depth – and their amplitudes decrease with depth. To make this statement we converted SLA variance into pressure variance using the hydrostatic equation. The combined annual and semi-annual harmonics at the eastern boundary ~~seasonal cycle off Angola as reconstructed using the annual and semi-annual harmonics~~ (Fig. 5 ~~(~~b,d~~,~~ and f~~)~~) show~~s~~ a similar structure at different depth with ~~maximum~~ maxima in austral autumn and spring, and a minimum in winter ~~and second maximum in spring~~. ~~But~~Nevertheless, the phases of the annual and semi-annual cycles change with depth at different rates (Fig. 6). With a phase shift of about 5 months, the annual harmonics at the surface and 500m depth are almost out-of-phase. The semi-annual harmonic is rather in-phase peaking about 1.5 month earlier at depth. This difference in the phase changes with depth can be associated with CTWs of certain baroclinic modes. Kopte et al. (2018) associated the annual and semi-annual cycles of the alongshore velocity from the mooring at 11°S with basin-mode resonance in the equatorial Atlantic of the fourth and second baroclinic modes, respectively (Brandt et al., 2016). Corresponding CTWs propagate along the African coast towards 11° S thereby impacting the local velocity and pressure fields. At the western boundary (Fig. 5 ~~(~~a,c~~,~~ and e~~)~~), the seasonal variability of the observed pressure time series is less pronounced. The combined annual and semi-annual harmonics explain only 12% of the total variance at the surface and are barely different from zero, considering ~~our~~ the uncertainty estimate for the amplitude. Seasonal variability of the surface pressure is decoupled from the pressure variability at depth, which supports the undercurrent character of the NBUC.~~.~~ The BP measurements at 300 m and 500 m depth, which are both located in the depth range of the NBUC, have annual and semi-annual harmonics of similar amplitude and phase (Fig. 5 d and f). The phase of the annual harmonic changes by 2 months between the surface and 300 m depth, the semi-annual harmonic by ~1 month and both peak later at depth (Fig. 5 b and d). At depth, seasonal pressure variations also become more important - at 500 m depth, for example, the annual and semi-annual harmonics explain up to 29%. This was consistently derived for 2-year subsets of the western boundary BP time series.

Annual and semi-annual harmonics of the individual pressure time series simulated ~~In~~ in the INALT01 model (grey shading in Fig. 5) agree quite well with the observations regarding the timing of the maxima and minima. On the other hand, there are large differences in the amplitudes: The model tends to overestimate the annual harmonic at the surface and generally underestimate seasonal variability ~~in general~~ at depth - especially at the western boundary ~~300 m depth~~ the seasonal cycle of the simulated BP at 300 m and 500m depth is almost non-existent.~~at the western boundary.~~

In ~~this study~~summary, for the seasonal variability at 11°S we observed that ~~estimate variations in the upper ocean geostrophic transport as a contribution to the AMOC from pressure differences across the basin. Based on the observations at 11° S, on seasonal time scales, we find~~ near the surface eastern boundary pressure variations ~~to~~ prevail ~~near the surface~~, whereas at 500 m depth the western and eastern boundary pressure variations are of similar importance. In the INALT01 model, the eastern boundary pressure variations dominate even more over western boundary ones.

5.2 Wind stress variability

Prevailing wind ~~stress~~s along 11° S ~~is northwestward~~are from southeast, which results in a mean ~~southward~~ meridional Ekman transport toward south. Using wind stress derived from ASCAT for the period 2013-2018 the mean and standard error of the meridional Ekman transport amounts to ~~it is~~ -11.7 ± ~~1~~0.9 Sv and for the full available period 2007-2018 ~~it is~~to -11.8 ± 0.6~~1.3~~ Sv. ~~For the CORE2b wind stress used as forcing for the 30-year INALT01 model run, we derive an~~The mean and standard error of the meridional Ekman transport derived from INALT01 wind stress ~~of~~ amounts to -10.~~8~~7 ± 0.~~5~~3 Sv. ~~While the Z~~zonal wind stress in the tropical South Atlantic varies on different time scales, ~~it~~ but is clearly dominated by seasonal variability. Periodograms of the Ekman transport ~~derived from~~based on ASCAT and INALT01~~CORE2b~~ wind stress (Fig. 7 ~~(~~a and ~~,~~b~~)~~) both show the strongest peaks at the frequency of the annual cycle. ~~The CORE2b winds do also show weak semi-annual variability, but only when considering the full time series from 1978-2009.~~ Note, that the two products cover very different periods and that their periodograms both also hint towards longer-term variability, whenever considering the full ~~available time series~~records.

The ~~Comparing~~ zonal wind stress anomalies at 11° S ~~from~~ for the two analyzed wind products for the overlapping years 2008-2009 (Fig. 7 ~~(~~c and ~~,~~d~~)~~) agree in the following characteristics~~, we find both products to agree on the following aspects~~: Seasonal wind variability is clearly more pronounced in the western part of the basin with zonal wind stress anomalies typically being westward (negative) in January to March – resulting in a weaker southward Ekman transport. In austral winter zonal wind stress anomalies are rather eastward (positive) and the southward Ekman transport is strongest - changing again towards the end of the year. For both wind products, the Ekman transport across 11° S is mainly governed by the seasonal cycle of the southeasterly trade winds (e.g. Philander & Pacanowski, 1986). However, there are also recognizable differences between both products: For 2008-2009, the mean and the monthly standard deviation of the Ekman transport at 11° S (not shown) are about 0.5 Sv larger for ASCAT than for INALT01~~CORE2b~~, respectively. Wind stress anomalies along 11° S reveal differences in its spatial structure, as well as in the course and amplitudes of its seasonal cycle (Fig. 7 ~~(~~c and ~~,~~d~~)~~).

5.3 Seasonal variability of the AMOC components at 11°S

As described in the methods, we ~~are~~ were able to estimate AMOC transport variations in the tropical South Atlantic from BP measurements over the period 2013-2018. Figure 8 displays the derived time series of T'_G, T'_{EK} and ~~, being~~ the sum of both components~~,~~ T'_{AMOC} at 11° S. The different versions of T'_G derived from 4 BPRs or from 2-3 BPRs complemented with the combined annual and semi-annual harmonics ~~from the fully equipped period~~ (Fig. 8(a), see section 4.1) show a general good agreement within the overlapping period. In the following sections, we analyzed the combined time series of $T'_{G\ EOFs\ 2\ BPRs}$ (07/2013 to 05/2014), $T'_{G\ EOFs\ 4\ BPRs}$ (05/2014 to 11/2015) and $T'_{G\ EOFs\ 2\ BPRs}$ (11/2015 to 03/2018; compare Fig. 8a) ~~In the following, we will use only a combined timeseries derived from all available BPR time series.~~

While ~~F~~from the BP observations we ~~can~~ could only derive anomalies of T_G ~~., In~~ in INALT01, ~~on the other hand~~however, we ~~can~~ could also calculate ~~also~~ mean values: The AMOC transport at 11° S ~~calculated from~~based on the ~~the velocity field in~~ INALT01 velocity field averaged over the whole model run (1978-2007) is $T_{AMOC\ SIM}$ = 14.1 ± 0.~~9~~ 5 Sv (mean and standard error). This is within the uncertainty range of 3 Sv for the AMOC estimate of 16.2 ~~± 3.0~~ Sv derived from a hydrographic ship section along 11° S in 1994 (Lumpkin & Speer, 2007).

Both, the T'_G and T'_{EK} time series and, hence, also T'_{AMOC}, show variability on different time scales, but are clearly dominated by seasonal variability ~~and, correspondingly, T'_{AMOC} is as well~~. M~~The m~~ean seasonal cycles of T'_G, T'_{EK} and T'_{AMOC} from observations and INALT01 ~~for the period 2013-2018, as well as from INALT01,~~ are shown in Fig. 9. ~~Despite having different products and different periods, we find the timing of the seasonal cycles in the observations and in INALT01 to be very similar for all components – especially, when considering possible interannual variations of the seasonal cycle.~~

T'_{EK} is characterized by a maximum southward transport in June-August and minimum southward transport in January-March, with the individual extrema slightly varying between ASCAT and INALT01~~CORE2b~~. Note again, that both products are averaged over different periods. The peak-to-peak amplitude of seasonal Ekman transport variations is 7.1 Sv for ASCAT wind stress~~s~~ ~~(over the period~~ 2007-2018; ~~(~~Fig. 9 ~~(~~c~~)~~) and 4.9 Sv for INALT01~~CORE2b~~ wind stress ~~for (~~1978-2009 ~~(~~; Fig. 9 ~~(~~d~~)~~). ~~Section 5.2 describes the differences in wind stress between both products in more detail. We can give an estimate of the~~ The seasonal cycles may vary from year to year as well as on longer time scales. Here, such variations are, for example, ~~interannual variability by showing~~estimated with the range of mean seasonal cycles calculated for running 5-year subsets of the available wind stress data~~:~~. While the timing of the seasonal cycle of T'_{EK} ~~does not change much~~is rather stable between different periods, ~~its amplitude changes, showing that~~the peak-to-peak amplitudes have a ~~of~~ range of 6-11 Sv for ASCAT and 2-8 Sv for INALT01~~CORE2b are possible~~.

The observed upper-ocean geostrophic transport anomaly (T'_G) shows a maximum northward transport in June, while minima occur in October and January with a weak secondary maximum ~~in between~~ in December. The two estimates, $T'_{G\ Points}$ and $T'_{G\ EOFs}$, ~~derived with~~referring to the two different methods, agree well in the timing of minima and maxima (Fig. 9 ~~(~~a~~)~~). However, the amplitude of the seasonal cycle of $T'_{G\ EOFs}$, which we ~~will be~~ consider~~ed~~ ~~as~~ to be the more realistic solution in the following, is about 2 Sv smaller than the corresponding amplitude of $T'_{G\ Points}$. A possible explanation for the difference

between the two estimates based on observations ~~will be~~ is given below~~, when discussing the vertical structure of the geostrophic transport per unit depth from simulations (Fig. 10).~~

Nevertheless, the seasonal cycles of both estimates based on observations, $T'_{G\ Points}$ and $T'_{G\ EOFs}$, are substantially more pronounced than that of $T'_{G\ SIM}$ derived directly from the velocity fields of the 30-year model run (Fig. 9 ~~(~~b~~)~~). The peak-to-peak amplitude of the seasonal cycle of $T'_{G\ SIM}$ ~~averaged~~ calculated over 30 years is 5.5 Sv, while amplitudes can range~~s~~ between 2-10 Sv when calculated for 5-year subsets. The peak-to-peak amplitude of $T'_{G\ EOFs}$ calculated over the observed 4.5 years is 12.2 Sv ~~averaged over the observed 4.5 years~~and thus larger than the model range~~,~~. Even when comparing the total range of possible seasonal cycles obtained by considering only single years, the observed values are just out of the range of the simulated values. ~~or between 10.6-14.2 Sv considering the standard errors, which is just out of the range of simulated values.~~ Regarding the timing of minima and maxima, the observed and simulated seasonal cycles of T'_G agree quite well (cf. Fig. 9 ~~(~~a and ~~,~~b~~)~~). The larger peak-to-peak amplitudes of the seasonal cycle of T'_G from observations (cf. Fig. 9a and b) ~~the observed upper-ocean geostrophic~~ as well as the ASCAT Ekman transports (cf. Fig. 9c and d) result in a larger seasonal cycle of T'_{AMOC} compared to $T'_{AMOC\ SIM}$ (cf. Fig. 9e and f).

~~Testing~~ In order to test our observational strategy ~~in INALT01~~, we compared the upper-ocean geostrophic transport anomaly derived directly from the simulated meridional velocity component ($T'_{G\ SIM}$) to ~~that~~ the one being derived from simulated BP time series. Using the full vertical resolution of the model when deriving ~~$V'_{G\ SIM\ P(z)}$ and $T'_{G\ SIM\ P(z)}$ (Fig. 10(a,b)) are calculated using the full vertical resolution of the model and, as expected,~~ $T'_{G\ SIM\ P(z)}$, we obtained good agreement with ~~agrees well with~~ $T'_{G\ SIM}$ as expected (Fig. 10a and b). ~~To resemble the observations, we also use piecewise linear interpolation between~~ Reducing the vertical resolution to the depths of the pressure observations at 0 m, 300 m, 500 m depth and using piecewise linear interpolation between those and ~~the~~ a 'level of no motion' at 1130m ($V'_{G\ SIM\ Points}$; $T'_{G\ SIM\ Points}$; Fig. 10 ~~(~~c and ~~,~~d~~)~~). ~~In INALT01, ,~~ we ~~find~~ found this method to miss certain parts of the vertical structure of $V'_{G\ SIM\ P(z)}$, and with that, to substantially overestimate the peak-to-peak amplitude of the seasonal cycle of $T'_{G\ SIM\ P(z)}$ by 6 Sv (Fig. 10 ~~(~~d~~)~~). While in the model a strong seasonal cycle is confined to the near-surface ocean, ~~using~~ linear interpolation between the surface and 300m artificially increases the seasonal signal in the layer from 50 to 250 m depth. ~~Another~~ To improve the approximation, another method ~~is~~ was applied that is based on a regression of the 1st and 2nd dominant vertical structure functions of $V'_{G\ SIM\ P(z)}$ onto the values at the 3 depth levels of pressure observations at 0 m, 300 m, 500 m depth ($T'_{G\ SIM\ EOFs}$; $V'_{G\ SIM\ EOFs}$, Fig. 10 ~~(~~e and ~~,~~f~~)~~) thereby relaxing the no-flow condition at 1130 m depth. As the first two EOFs of $V'_{G\ SIM\ P(z)}$ explain 99% of the variance contained in $V'_{G\ SIM\ P(z)}$, $T'_{G\ SIM\ EOFs}$ agrees well with $T'_{G\ SIM\ P(z)}$ in INALT01 (Fig. 10 ~~(~~f~~)~~). However, ~~from comparing~~ the comparison of the observed BP time series with the BP simulated in INALT01 (Fig. 4), ~~we learned~~shows that the model tends to underestimate the seasonal pressure variability at depth (see section 5.1) leaving some uncertainty regarding the vertical structure of V'_G in reality.

Figure 11 compares the mean seasonal cycles of V'_G from observations for the two different methods. Using the vertical structure from the EOFs of $V'_{G\ SIM\ P(Z)}$ from INALT01 does especially reduce the amplitude of the subsurface variability (50-

200 m). In this depth range the transition from negative to positive transport anomalies also shifts from April to March. At larger depths, differences between both methods are the result from ~~the fact that~~ $V'_{G\ Points}$ ~~is~~ being ~~constraint~~ constrained by a level of no motion at 1130 m, while $V'_{G\ EOFs}$ is not. However, independent of the applied method, the peak-to-peak amplitude of the seasonal cycle of T'_G from observations (Fig. 9 ~~(~~a~~)~~) remains to be substantially larger than that from INALT01.

For ~~This means, that for~~ the period 2013-2018, the geostrophic contribution to the seasonal cycle of the AMOC at 11° S, as we observed it, exceeds the Ekman contribution almost by a factor of 2 (cf. Fig. 9 ~~(~~a and ~~,~~c~~)~~). In INALT01, on the other hand, averaged over the 30-year model run, the geostrophic and Ekman contributions are of similar magnitude (Fig. 9 ~~(~~b and ~~,~~d~~)~~). The seasonal cycles of both contributions vary substantially between years (calculated for 5-year subsets of the model run) – e.g. 2-10 Sv for $T'_{G\ SIM}$ from INALT01, 2-8 Sv for T'_{EK} from INALT01~~CORE2b~~ or 6-11 Sv for T'_{EK} from ASCAT - ~~which means that~~hence there is a modulation of the ratios of both contributions on interannual time scales. However, even when considering the ~~standard errors calculated for~~uncertainties of the seasonal cycle of $T'_{G\ Points}$ or $T'_{G\ EOFs}$ ~~over 2013-2018~~ (Fig. 9 ~~(~~a~~)~~) and the range of possible mean seasonal cycles of $T'_{G\ SIM}$ calculated for ~~5-year~~ subsets of the model run ~~period 1978-2007~~ (Fig. 9 ~~(~~b~~)~~), the observed values are significantly larger than simulated ones.

5.4 Dynamics of the seasonal cycle at 11°S

In order to better understand the mechanisms that set the seasonal cycle of T'_{AMOC} at 11° S, we investigated the longitudinal structure of the geostrophic velocity field and ~~the geostrophic~~ transport along that section in INALT01. We ~~are~~ were able to distinguish three different regimes – the NBUC, the Western Basin Interior and the Eastern Basin - all showing seasonal variability of similar magnitude (Fig. 12).

The mean seasonal cycle of the NBUC, as calculated for the 30-year INALT01 model run, has its maximum in April, minimum in November and a peak-to-peak amplitude of 10 Sv (Fig. 12 ~~(~~b~~)~~). Peak-to-peak amplitudes of up to 15 Sv ~~are~~ can be found in 5-year subsets of the model time series. Having a mooring array installed off the coast off Brazil measuring the Western Boundary Current system there (~~Schott et al., 2005;~~e.g. Hummels et al., 2015; see section 2.4), ~~allows~~ allowed us to directly compare the seasonal variability of the NBUC in INALT01 with observations. The seasonal cycle of the NBUC in INALT01 agrees quite well with the seasonal cycle observed in recent years – regarding the peak-to-peak amplitude (7.6 Sv in 2000-2004 and 7 Sv in 2013-2018) and the timing of maximum and minimum transports (Fig. 13 ~~(~~b~~)~~). During the earlier deployment period 2000-2004 there ~~is~~ was a stronger semi-annual cycle creating a secondary minimum in March, which ~~is~~ was neither found in the observations during 2013-2018 nor in INALT01.

In INALT01, the contribution of the NBUC to the AMOC on seasonal time scales is largely compensated by the flow in the western basin interior. The seasonal cycle of the geostrophic transport per unit depth in the western basin interior is of similar strength and vertical structure, but opposing sign to the one of the NBUC (cf. Fig. 12 ~~(~~a and ~~,~~c~~)~~). In the western basin interior, the vertically integrated upper-ocean geostrophic velocity is mainly associated with an annual harmonic and likely related to a strong seasonal cycle in the local wind stress curl (Fig. 14~~(a)~~). The annual harmonic of the wind stress curl exhibits relatively

large amplitudes over the region (~~15~~10° W to 34.55° W) and a westward phase propagation (not shown). ~~In the same region, below the Ekman layer, the phases of the annual harmonic of the meridional velocity show a low baroclinic mode structure (Fig. 14(b)).~~

As the contributions of the NBUC and western basin interior seasonal cycles to the AMOC tend to cancel ~~out~~ each other out, in INALT01, seasonal variability of the upper-ocean geostrophic transport at 11° S is mainly set in the eastern basin (Fig. 12 ~~(~~f~~)~~). Both, the vertically integrated upper-ocean geostrophic velocity and the wind stress curl (Fig. 14), exhibit strong seasonal variability throughout most of the eastern basin. However, the largest amplitudes of the annual and semi-annual harmonics of the vertically integrated upper-ocean geostrophic velocity are found near the eastern boundary, east of 12°E, where seasonal variability in the wind stress curl is weak.

~~Away from the Ekman layer, the annual and semi annual harmonics of the meridional velocity in the eastern basin are dominated by westward and upward phase propagation (Fig. 14(b,c)). This suggests the existence of westward and downward propagating Rossby beams likely related to remote equatorial forcing (e.g. Chu et al., 2007).~~

~~In addition to a westward, upward propagation, the phases of the annual and semi annual harmonics of the meridional velocity in the eastern basin also show a vertical structure along the continental slope and sustained into the eastern basin interior. In INALT01, Rossby waves dominate the meridional velocity east of 5° W, but largely do not cross the Mid-Atlantic Ridge into the western basin indicated by the minimum in the annual and semi-annual harmonics in mid-basin (Fig. 14).~~

From this analysis, we conclude that ~~the seasonal variability of the geostrophic contribution to the AMOC at 11° S mainly results from the oceanic adjustment to local and remote wind forcing. In INALT01,~~ a compensation between the NBUC and western basin interior results in a ~~minor~~ major contribution of the upper-ocean geostrophic transport ~~from~~ of the ~~western~~ eastern basin to the AMOC transport ~~compared to a major contribution from the eastern basin~~ on seasonal time scales. As described in section 5.1, however, the model tends to underestimate the seasonal pressure variability at 300 m and 500 m depth – especially at the western boundary. This leaves some uncertainty in the relative importance of western and eastern basin contributions to ~~total~~ the seasonal AMOC variability in reality.

6 Summary and discussion

In this study, we used bottom pressure observations on both sides of the basin at 300 m and 500 m depth, combined with satellite measurements of sea level anomalies, different wind stress products and model results, to estimate the upper-ocean geostrophic and Ekman transport contributions to AMOC variability at 11° S over the period 2013-2018.

The use of bottom pressure measurements to compute basin-wide integrated northward transports is not straightforward: Firstly, the sensors experience instrumental drifts, which limits the BPRs capabilities to recover variability on longer time scales. Secondly, the deployment depth is not precisely known, which only allows ~~only~~ the calculation of transport anomalies~~,~~

~~but not of mean values~~. We ~~find~~ found the available BP time series at 11° S to be ~~just~~ sufficiently long ~~enough~~ to investigate the seasonal variability in ~~that~~ the region~~.~~, but, clearly, longer time series will allow us to refine these estimates in the future.

At 11° S, seasonal variability is strong in most of the ~~all of the~~ time series presented in this study. After removing tides with periods shorter than 35 days, the combined annual and semi-annual harmonics explain ~~most~~ a large part of the variability at the eastern boundary – from 60% at the surface to 44% at 500 m depth. We ~~find~~ found hints towards a baroclinic structure in the annual and semi-annual harmonics of the pressure time series at the eastern boundary (Fig. 6), which could be related to CTWs of specific baroclinic modes that can travel from the equator towards 11° S along the African coast thereby impacting the local pressure and velocity fields. ~~The observed annual harmonic of the alongshore velocity at 11° S presented in Kopte et al. (2018) also exhibits a flow reversal between the surface and ~ 50 m, while the semi-annual harmonic is instead characterized by a more gradual change with depth. They confirm the association of the annual and semi-annual cycles with basin mode resonance in the equatorial Atlantic of the fourth and second baroclinic modes, respectively (Brandt et al., 2016). CTWs of this baroclinic structure can travel along the African coast towards 11° S thereby impacting the local velocity and pressure fields.~~

~~The region off Angola is known to be dominated by CTWs not only on seasonal, but on intraseasonal to interannual time scales (e.g. Bachèlery et al., 2016; Illig et al., 2018a,b; Kopte et al., 2018). The periodograms of SLA at the eastern boundary exhibit peaks at 90 days and 120 days. The peaks at periods of 90 days and 120 days have also been found by Kopte et al. (2018) in velocity time series from moored observations at 11° S off Angola. Based on numerical experiments, Bachèlery et al. (2016) showed that SLA variability along the African coast is on intraseasonal time scales (T<105 days) primarily driven by local atmospheric forcing, while energetic signals at periods >120 days are mostly explained by equatorial forcing. Further, Polo et al. (2008) suggested that the intraseasonal variability is related to year-to-year variations of the seasonal cycle. Note that there is enhanced spectral energy at periods of 1.5 – 2.5 years in the eastern boundary SLA, which is also present when considering the full time series from 1993–2018 (Fig. 4(b)).~~

At the western boundary, seasonal pressure variability is weaker with ~~, but~~ its relative importance compared to other variability ~~increases~~ increasing with depth - the annual and semi-annual harmonics explain about 10% of the variability at the surface and 30% at 500 m depth. The seasonal variability of the zonally integrated geostrophic velocity anomaly in the upper 300 m is, therefore, mainly controlled by pressure variations at the eastern boundary, while at 500 m depth contributions from the western and eastern boundaries are similar. Annual ~~und~~ and semi-annual harmonics at the western boundary also exhibit a vertical structure as seasonal variability at the surface is decoupled from the pressure variability at 300 m and 500 m depth. Based on geostrophic velocity fields from hydrographic measurements, studies like Silveira et al. (1994) or Stramma et al. (1995) already stated that the WBC system at 11° S includes an ~~pronounced~~ energetic undercurrent, the NBUC, with weak or reversed flow above. From moored observations, Schott et al. (2005) showed strong gradients in the amplitude of the annual harmonic in the upper few hundred meters of the water column (their Fig. 11a) suggesting a decoupling of the variability at the surface from the subsurface.~~above which higher current variability was observed. Further, the BP periodograms show a peak at 70 days~~

~~(Fig. 4(c,e)), which is likely related to the DWBC eddies described by Dengler et al. (2004) also influencing the upper water column.~~

Over the period 2013-2018, the upper-ocean geostrophic transport variations derived from pressure differences across the basin, are dominated by seasonal variability – with a peak-to-peak amplitude of 12-14 Sv, depending on the method used to approximate its vertical structure. The peak-to-peak amplitude of the mean seasonal cycle of the Ekman transport is 7 Sv and of the resulting AMOC transport 14-16 Sv. For the Subtropics, recent estimates of the peak-to-peak amplitude of the mean seasonal cycle of the AMOC range from 4.3 Sv at 26.5°N (2004-2017; Frajka-Williams et al., 2019) to 13 Sv at 34.5°S (2014-2017; Kersale et al., 2020). ~~From moored observations of the Western Boundary Current system off Brazil (updated from Schott et al., 2005; Hummels et al., 2015), we obtain a peak-to-peak seasonal variability of the NBUC of 7 Sv.~~

The output of the OGCM INALT01 was compared to the observed characteristics of the seasonal cycles of the AMOC, its components as well as the NBUC. It reproduces the seasonal cycles of the NBUC as observed in recent years with current meter moorings and of the Ekman transport across 11° S as derived from ASCAT winds. However, this comparison also reveals model-observation discrepancies regarding seasonal variability in the bottom pressure fields and the resulting geostrophic transport variations:

~~The observed seasonal cycles of the AMOC, its components as well as the NBUC are in general good agreement with the output of the OGCM INALT01.~~

~~Nevertheless, there are some notable differences:~~

- The INALT01 model tends to underestimate the seasonal bottom pressure variability at ~~depth (~~300 m and 500 m~~)~~, especially at the western boundary. This translates into the vertical structure of the simulated geostrophic transport variations, which is also used for the calculation of the observational estimate (method 2) ~~and, therefore, adds~~adding to its uncertainty.
- In the observations, the geostrophic contribution to seasonal AMOC variability exceeds the Ekman contribution by almost a factor of 2, while in INALT01, averaged over the 30-year model run, or in earlier studies based on models (e.g. Zhao & Johns, 2014), the contributions are similar. ~~About equal geostrophic and Ekman contributions were also observed at other latitudes (at 26° N in Kanzow et al., 2010; at 34.5° S in Dong et al., 2014) or identified in earlier studies based on models (e.g. Zhao & Johns, 2014).~~ Even when considering the ~~standard errors~~multi-year variations ~~calculated for~~of the seasonal cycle of T_G' over 2013-2018 (Fig. 9(a)) and the total range of possible ~~mean~~ seasonal cycles of $T_{G\,SIM}'$ calculated for ~~5-year~~ subsets of the model run period 1978-2007 (Fig. 9(b)), the observed values are significantly larger than the simulated values.
- The ratios of the NBUC and AMOC seasonal amplitudes are different between the observations (<1) and the model (>1).

In the model, seasonal ~~AMOC~~ upper-ocean geostrophic transport variability at 11° S is governed by the variability in the eastern basin. The seasonal cycle of the simulated upper-ocean geostrophic transport in the western basin becomes comparable small due to a compensation of the western basin interior and the NBUC transports. This could be explained by an almost equilibrium response of the circulation in the western basin at low baroclinic modes to the wind stress curl (e.g. Döös, 1999). Locally wind-forced annual Rossby waves would travel westward and after arriving at the western boundary directly force WBC variability. The seasonal variability in the eastern basin is instead forced by the local wind stress curl and, additionally, by Rossby waves radiated from the eastern boundary via poleward propagation of seasonal CTWs (e.g. Brandt et al., 2016; Kopte et al., 2018). Similar Rossby-wave radiation from the eastern boundary has been reported for the tropical North Atlantic (e.g. Chu et al., 2007) and proposed to be one of the main mechanisms for seasonal variations in the geostrophic transport there (e.g. Hirschi et al., 2006; Zhao & Johns, 2014).

~~where the annual and semi-annual harmonics of the meridional velocity is dominated by westward and upward phase propagation (Fig. 14(b,c)). This can be related to equatorial forcing resulting finally into long Rossby waves to be radiated from the Angolan continental slope and travelling westward into the basin interior. Similar Rossby wave radiation from the eastern boundary have been reported for the tropical North Atlantic (e.g. Chu et al., 2007) and proposed to be one of the main mechanisms for seasonal variations in the geostrophic transport there (e.g. Hirschi et al., 2006; Zhao & Johns, 2014).~~

~~In addition to a westward propagation, the phases of the annual and semi-annual harmonics of the meridional velocity in the eastern basin also show a specific vertical structure. We interpret this to be related to the baroclinic structures of seasonal CTWs (e.g. fourth mode for annual cycle; Brandt et al., 2016; Kopte et al., 2018) arriving at 11° S, being radiated as Rossby waves with a similar baroclinic structure.~~

~~Concurrently, the seasonal variability of the NBUC is mainly compensated by a low baroclinic mode signal in the western basin interior. Being related to a strong seasonal cycle of the wind stress curl in the western basin, we interpret this signal as locally forced Rossby waves. In an early model study, Döös (1999) described the influence of long Rossby waves on the seasonal cycle in the western tropical Atlantic. Also, Schott et al. (2005) suggested the seasonal cycles of the NBUC and DWBC at 11° S to be a response to interior wind forcing, occurring as a first baroclinic mode Rossby wave. Locally wind-forced seasonal Rossby waves would travel westward and after arriving at the western boundary directly force WBC variability.~~

The compensation between the western basin interior and the NBUC on seasonal time scales found in INALT01 results in a minor contribution of the western basin compared to ~~the contribution from~~ the eastern basin ~~to~~ and limits the importance of the NBUC for AMOC variability on seasonal time scales. ~~But~~However, ~~it is also subject to numerous uncertainties: In~~in this study we ~~found~~ found that INALT01 tends to underestimate seasonal variability ~~in the central water layers~~at 300m and 500m off Brazil. In two different model studies, Rodrigues et al. (2007) and Silva et al. (2009), related seasonal variability in the NBUC to seasonal variations in the bifurcation region of the South Equatorial Current. Thus, the phases of the annual and semi-annual harmonics of the NBUC may not ~~be~~ simply be set by the response to the local wind curl forcing in the western

basin at 11° S, ~~they~~ but may also depend on the wind curl forcing farther south and associated equatorward signal propagation along the western boundary.

We conclude that the seasonal variability of the geostrophic contribution to the AMOC at 11° S is mainly wind-forced, as it is modulated by oceanic adjustment to local and remote wind forcing. While some of the uncertainties of our analysis result from the technical aspects of the observational strategy or processes being not properly represented in the model, our results indicate, that uncertainties in the wind forcing are particularly relevant for AMOC estimates in the tropical South Atlantic. Differences between wind products are an important source of uncertainty for estimates of the AMOC and its variability. Especially, when comparing estimates of AMOC strength and variability between different projects, latitudes or from observations and models, the choice of wind product is crucial.

This study adds to the overall understanding of local and shorter-term AMOC variations, which is important for estimating the significance of long-term AMOC changes and, thus, for the detectability of its meridional coherence. To predict the long-term behavior of the AMOC and its impacts, continuous observations from purposefully designed arrays are ~~needed~~ required in different key locations. We would like to argue that the observational program at 11° S, if continued into the future, has potential for monitoring long-term AMOC changes. As ~~T~~the western tropical Atlantic ~~being~~ is a crossroad for the different branches of the AMOC and a region with high signal-to-noise ratios, ~~makes~~ 11° S is a good place to monitor AMOC variations. Having a sustainable AMOC observing system there, linking northern and southern AMOC variability, would contribute to the general understanding of related mechanisms. There is potential ~~in using the setup of~~to use the BPRs for investigating longer-term AMOC variability. While progress is made in solving the problems of bottom pressure sensors on longer time scales (e.g. Kajikawa & Kobata, 2014; Worthington et al., 2019), the advantage of our method is that the BPRs are less expensive and easier to deploy than full-height mooring arrays. Learning from the use of long-term PIES arrays at 47° N (Roessler et al., 2015) or 34.5° S (e.g. Meinen et al. 2018), we think that the travel times derived from the PIES installed off Brazil could add information to or reduce the uncertainty of our results. Additionally, we can fall back on more than 20 years of shipboard hydrographic measurements in the tropical South Atlantic – at the western (e.g. Hummels et al., 2015; Herrford et al., 2017) and eastern boundary (e.g. Tchipalanga et al., 2018). Ongoing work includes combining all of these hydrographic measurements to extend the time series of the WBC system and AMOC at 11° S back into the 1990s.

Author contribution

The methodology was first proposed T.K., then further developed and conceptualized by J.H. and P.B. P.B. and R.H. raised the project funding and, together with M.A., administered the project. The investigation was made by J.H., supervised and validated by P.B. and T.K. J.H. processed the observational data, performed all analyses, drafted the manuscript and designed the figures. J.V.D. developed INALT01 and performed the simulations. R.H. calculated and provided the NBUC transport time series. All authors contributed to the discussion of the results or the review and editing of the manuscript.

Disclaimer

The authors declare that they have no conflict of interest.

Acknowledgements

This study was funded by the Deutsche Bundesministerium für Bildung und Forschung (BMBF) as part of the projects RACE (03F0651B, 03F0729C, 03F0824C), SACUS (03G0837A) and BANINO (03F0795A, 03F0795C), by the EU H2020 under grant agreement 817578 TRIATLAS project and by the Deutsche Forschungsgemeinschaft (DFG) through funding of Meteor cruises. We thank captains and crews of the R/V Meteor and R/V Sonne, as well as our technicians for the assistance during the shipboard and moored station work. Data sets described in section 2.1 are available through https://doi.pangaea.de/ SLA data was distributed by the E.U. Copernicus Marine Service Information. INALT01 was developed at GEOMAR, with details of its configuration and access to data available at https://www.geomar.de/forschen/fb1/fb1-od/ocean-models/inalt01~~www.geomar.de/en/research/fb1/fb1-od/ocean-models/inalt01/~~. J.V.D acknowledges funding from the Helmholtz Association and the GEOMAR Helmholtz Centre for Ocean Research Kiel (grant IV014/GH018). We would like to thank G. Krahmann and M. Dengler for helpful discussions, and are very greatful for the constructive comments by two anonymous reviewers.

References

Bachèlery, M.-L., Illig, S., and Dadou, I.: Interannual variability in the South-East Atlantic Ocean, focusing on the Benguela Upwelling System: Remote versus local forcing, J. Geophys. Res. Oceans, 121, 284–310, doi:10.1002/2015JC011168, 2016.

Bentamy, A. and Croizé-Fillon, D.~~C.~~: Gridded surface wind fields from Metop/ASCAT measurements, International Journal of Remote Sensing, 33(6), 1729-1754. Publisher's official version: doi:10.1080/01431161.2011.600348, Open Access version: https://archimer.ifremer.fr/doc/00043/15440/, 2012.

Biastoch, A., Böning, C. W., and Lutjeharms, J. R. E.: Agulhas leakage dynamics affects decadal variability in Atlantic overturning circulation, Nature, 456, 489–492, 2008.

Brandt, P., Claus, M., Greatbatch, R. J., Kopte, R., Toole, J. M., Johns, W. E., and Böning, C. W.: Annual and semiannual cycle of equatorial Atlantic circulation associated with basinmode resonance. J. Phys. Oceanogr., 46, 3011–3029, https://doi.org/10.1175/JPO-D-15-0248.1, 2016.

Buckley, M. W. and Marshall, J.: Observations, inferences, and mechanisms of the Atlantic Meridional Overturning Circulation: A review, Rev. Geophys., 54, doi:10.1002/2015RG000493, 2016.

Chidichimo, M. P., Kanzow, T., Cunningham, S. A., Johns, W. E., and Marotzke, J.: The contribution of eastern-boundary density variations to the Atlantic meridional overturning circulation at 26.5° N. Ocean Sci., 6, 475–490, doi: 10.5194/os-6-475-2010, 2010.

Chu, P. C., Ivanov, L. M., Melnichenko, O. V., and Wells, N. C.: On long baroclinic Rossby waves in the tropical North Atlantic observed from profiling floats, J. Geophys. Res., 112, C05032, doi:10.1029/2006JC003698, 2007.

Codiga, D.L.: Unified Tidal Analysis and Prediction Using the UTide Matlab Functions. Technical Report 2011-01. Graduate School of Oceanography, University of Rhode Island, Narragansett, RI. 59pp. ftp://www.po.gso.uri.edu/pub/downloads/codiga/pubs/2011Codiga-UTide-Report.pdf, 2011.

Cunningham, S. A., Kanzow, T., Rayner, D., Baringer, M. O., Johns, W. E., Marotzke, J., Longworth, H. R., Grant, E. M., Hirschi, J. J.-M., Beal, L. M., Meinen, C. S., Bryden, H. L.: Temporal variability of the Atlantic meridional overturning circulation at 26.5° N, Science, 317, 935–938. doi:10.1126/science.1141304, 2007.

Cunningham, S. A.: RRS Discovery Cruise D334, 27 Oct-24 Nov 2008. RAPID Mooring Cruise Report, 2009.

Dengler, M., Schott, F. A., Eden, C., Brandt, P., Fischer, J., and Zantopp, R. J.: Break-up of the Atlantic deep western boundary current into eddies at 8 degrees S, Nature, 432(7020), 1018–1020, 2004.

~~Dong, S., Baringer, M. O., Goni, G. J., Meinen, C. S., and Garzoli, S. L.: Seasonal variations in the South Atlantic Meridional Overturning Circulation from observations and numerical models, Geophys. Res. Lett., 41, 4611–4618, doi:10.1002/2014GL060428, 2014.~~

Donohue, K. A., Watts, D. R., Tracey, K. L., Greene, A. D., and Kennelly, M.: Mapping circulation in the Kuroshio Extension with an array of current and pressure recording inverted echo sounders, J. Atmos. Ocean. Technol., doi:10.1175/2009JTECHO686.1, 2010.

Döös, K.: Influence of the Rossby waves on the seasonal cycle in the tropical Atlantic, J. Geophys. Res., 104(C12), 29591–29598, doi:10.1029/1999JC900126, 1999.

Durgadoo, J. V., Loveday, B. R., Reason, C. J. C., Penven, P., and Biastoch, A.: Agulhas leakage predominantly responds to the Southern Hemisphere westerlies, J. Phys. Oceanogr., 43(10), 2113–2131, 2013.

Frajka-Williams, E., Lankhorst, M., Koelling, J., and Send, U.: Coherent circulation changes in the Deep North Atlantic from 16° N and 26° N transport arrays. J. Geophys. Res., 123. doi:10.1029/ 2018JC013949, 2018.

Frajka-Williams, E., I. J. Ansorge, J. Baehr, H. L. Bryden, M. P. Chidichimo, S. A. Cunningham, G. Danabasoglu, S. Dong, K. A. Donohue, S. Elipot, P. Heimbach, N. P. Holliday, R. Hummels, L. C. Jackson, J. Karstensen, M. Lankhorst, I. A. Le Bras, M. S. Lozier, E. L. McDonagh, C. S. Meinen, H. Mercier, B. I. Moat, R. C. Perez, C. G. Piecuch, M. Rhein, M. A. Srokosz, K. E. Trenberth, S. Bacon, G. Forget, G. Goni, D. Kieke, J. Koelling, T. Lamont, G. D. McCarthy, C. Mertens, U. Send, D. A. Smeed, S. Speich, M. van den Berg, D. Volkov, and C. Wilson: Atlantic Meridional Overturning Circulation: Observed transport and variability, Frontiers in Marine Science, 6:260, doi: 10.3389/fmars.2019.00260, 2019.

Hansen, B., Larsen, K., Hátún, H., and Østerhus, S.: A stable Faroe Bank Channel overflow 1995-2015, Ocean Sci., 12, 1205–1220, doi:10.5194/os-12-1205-2016, 2016.

Herrford, J., Brandt, P., and Zenk, W.: Property Changes of Deep and Bottom Waters in the western tropical Atlantic. Deep-Sea Res. I, 124, 103-125, 2017.

Hirschi, J., Baehr, J., Marotzke, J., Stark J., Cunningham, S., and Beismann, J.-O.: A monitoring design for the Atlantic meridional overturning circulation, Geophys. Res. Lett., 30, 1413, doi:10.1029/2002GL016776, 7, 2003.

Hirschi, J.J., Killworth, P.D., and Blundell, J.R.: Subannual, Seasonal, and Interannual Variability of the North Atlantic Meridional Overturning Circulation. J. Phys. Oceanogr., 37, 1246–1265, https://doi.org/10.1175/JPO3049.1, 2006.

Hummels, R., Brandt, P., Dengler, M., Fischer, J., Araujo, M., Veleda, D., and Durgadoo, J. V.: Interannual to decadal changes in the western boundary circulation in the Atlantic at 11° S, Geophys. Res. Lett., 42, doi:10.1002/2015GL065254, 2015.

Illig, S., Cadier, E., Bachèlery, M.-L., and Kersale, M.: Subseasonal coastal-trapped wave propagations in the southeastern Pacific and Atlantic Oceans: 1. A new approach to estimate wave amplitude. J. Geophys. Res., 123, 3915–3941, doi:10.1029/2017JC013539, 2018a.

Illig, S., Bachèlery, M.-L. and Cadier, E.: Subseasonal coastal-trapped wave propagations in the southeastern Pacific and Atlantic Oceans: 2. Wave characteristics and connection with the equatorial variability. J. Geophys. Res., 123, 3942–3961, doi:10.1029/2017JC013540, 2018b.

Imbol Koungue, R. A., S. Illig, and M. Rouault: Role of interannual Kelvin wave propagations in the equatorial Atlantic on the Angola Benguela Current system. J. Geophys. Res. Oceans, 122, 4685–4703, https://doi.org/10.1002/2016JC012463,2017.

Jochumsen, K., Moritz, M., Nunes, N., Quadfasel, D., Larsen, K. M. H., Hansen, B., Valdimarsson, H., and Jonsson, S.: Revised transport estimates of the Denmark Strait overflow, J. Geophys. Res. Oceans, 122, 3434– 3450, doi:10.1002/2017JC012803, 2017.

Johns, W. E., Kanzow, T., and Zantopp, R.: Estimating ocean transports with dynamic height moorings: An application in the Atlantic Deep Western Boundary Current at 26◦N. Deep-Sea Res. I, 52(8), 1542–1567. doi:10.1016/j.dsr.2005.02.002, 2005.

Johns, W. E., Baringer, M. O., Beal, L. M., Cunningham, S. A., Kanzow, T., Bryden, H. L., Hirschi, J.J., Marotzke, J., Meinen, C.S., Shaw, B., and Curry, R.: Continuous, Array-Based Estimates of Atlantic Ocean Heat Transport at 26.5° N. J. Climate, 24, 2429–2449, doi:10.1175/2010JCLI3997.1, 2011.

Kajikawa, H., and Kobata, T.: Reproducibility of calibration results by 0-A-0 pressurization procedures for hydraulic pressure transducers. Meas. Sci. Technol., doi:10.1088/0957-0233/25/1/015008, 2014.

Kanzow, T., Flechtner, F., Chave, A., Schmidt, R., Schwintzer, P., and Send, U.: Seasonal variation of ocean bottom pressure derived from Gravity Recovery and Climate Experiment (GRACE): Local validation and global patterns. J. Geophys. Res., 110, C09001. doi:10.1029/2004JC002772, 2005.

Kanzow, T., Send, U., Zenk, W., Chave, A. D., and Rhein, M.: Monitoring the integrated deep meridional flow in the tropical North Atlantic: long-term performance of a geostrophic array. Deep-Sea Res. I, 53, 528–546, 2006.

Kanzow, T., Cunningham, S. A., Rayner, D., Hirschi, J. J.-M, Johns, W. E., Baringer, M. O., Bryden, H. L., Beal, L. M., Meinen, C. S., and Marotzke, J.: Observed flow compensation associated with the MOC at 26.5◦N in the Atlantic. Science, 317(5840), 938–941. doi:10.1126/science.1141293, 2007.

Kanzow, T., Send, U., and McCartney, M.: On the variability of the deep meridional transports in the tropical North Atlantic. Deep-Sea Res. I, 55, 1601-1623, doi: 10.1016/j.dsr.2008.07.011, 2008.

Kanzow, T., Cunningham, S. A., Johns, W. E., Hirschi, J. J., Marotzke, J., Baringer, M. O., Meinen, C. S., Chidichimo, M. P., Atkinson, C., Beal, L. M., Bryden, H. L., and Collins, J.: Seasonal Variability of the Atlantic Meridional Overturning Circulation at 26.5° N. J. Climate, 23, 5678–5698, doi:10.1175/2010JCLI3389, 2010.

Kersalé, M., C. S. Meinen, R. C. Perez, M. Le Henaff, D. Valla, T. Lamont O. T. Sato, S. Dong, T. Terre, M. van Caspel, M. P. Chidichimo, M. van den Berg, S. Speich, A. R. Piola, E. J. D. Campos, I. Ansorge, D. L. Volkov, R. Lumpkin, and S. Garzoli: Highly Variable Upper and Abyssal Overturning Cells in the South Atlantic, Science Advances, 6, eaba7573, 10.1126/sciadv.aba7573, 2020.

Kolodziejczyk, N., Reverdin, G., Gaillard, F., and Lazar, A.: Low-frequency thermohaline variability in the Subtropical South Atlantic pycnocline during 2002–2013, Geophys. Res. Lett., 41, 6468–6475, 2014.

Kopte, R., Brandt, P., Dengler, M., Tchipalanga, P. C. M., Macuéria, M., and Ostrowski, M.: The Angola Current: Flow and hydrographic characteristics as observed at 11° S, J. Geophys. Res. Oceans, 122, 1177– 1189, doi:10.1002/2016JC012374, 2017.

Kopte, R., Brandt, P., Claus, M., Greatbatch, R. J., and Dengler, M.: Role of equatorial basin-mode resonance for the seasonal variability of the Angola Current at 11° S, J. Phys. Oceanogr., 48, 261–281, 2018.

Large, W. G., and Yeager S. G. (2009). The global climatology of an interannually varying air-sea flux data set, Clim. Dyn., 33, 341–364, doi:10.1007/s00382-008-0441-3, 2009.

Lavin, A., Bryden, H. L., and Parilla, G.: Meridional transport and heat flux variations in the subtropical North Atlantic. Global Atmos. Ocean Sys., 6, 269-293, 1998.

Le Bars, D., Durgadoo, J. V., Dijkstra, H. A., Biastoch, A., and De Ruijter, W. P. M.: An observed 20-year time series of Agulhas leakage, Ocean Sci., 10, 601–609, doi:10.5194/os-10-601-2014, 2014.

Lozier, M. S., Li, F., Bacon, S., Bahr, F., Bower, A. S., Cunningham, S. A., de Jong, M. F., de Steur, L., DeYoung, B., Fischer, J., Gary, S. F., Greenan, N. J. W., Holliday, N. P., Houk, A., Houpert, L., Inall, M. E., Johns, W. E., Johnson, H. L., Johnson, C., Karstensen, J., Koman, G., LeBras, I. A., Lin, X., Mackay, N., Marshall, D. P., Mercier, H., Oltmanns, M., Pickart, R. S., Ramsey, A. L., Rayner, D., Straneo, F., Thierry, V., Torres, D. J., Williams, R. G., Wilson, C., Yang, J., Yashayaev, I., and Zhao, J.: A Sea Change in Our View of Overturning in the Subpolar North Atlantic. Science, doi: 10.1126/science.aau6592, 2019.

Lumpkin, R., and Speer, K.: Large-Scale Vertical and Horizontal Circulation in the North Atlantic Ocean. J. Phys. Oceanogr., 33, 1902–1920, 2003.

Lumpkin, R., and Speer, K.: Global ocean meridional overturning. J. Phys. Oceanogr., 37, 2550–2562, 2007.

Madec, G.: NEMO ocean engine, Note du Pole de modelisation, No. 27. Inst. Pierre-Simon Laplace (IPSL), France, 2008.

McCarthy, G. D., Smeed, D. A., Johns, W. E., Frajka-Williams, E., Moat, B. I., Rayner, D., Baringer, M. O., Meinen, C. S., Collins, J., Bryden, H. L.: Measuring the Atlantic meridional overturning circulation at 26° N. Prog. Oceanogr. 130, 91–111.doi:10.1016/j.pocean.2014.10.006, 2015.

Meinen, C. S., Johns, W. E., Garzoli, S. L., van Sebille, E., Rayner, D., Kanzow, T., and Baringer, M. O.: Variability of the Deep Western Boundary Current at 26.5° N during 2004-2009, Deep Sea Res. II, 85, 154-168, doi:10.1016/j.dsr2.2012.07.036, 2013.

Meinen, C. S., Garzoli, S. L., Perez, R. C., Campos, E., Piola, A. R., Chidichimo, M.-P., Dong, S., and Sato, O. T.: Characteristics and causes of Deep Western Boundary Current transport variability at 34.5° S during 2009-2014, Ocean Sci., 175-194, doi:10.5194/os-13-175-2017, 2017.

Meinen, C. S., Speich, S., Piola, A. R., Ansorge, I., Campos, E., Kersale, M., Terre, T., Chidichimo, M.-P., Lamont, T., Sato, O. T., Perez, R. C., Valla, D., van den Berg, M., Le Henaff, M., Dong, S., and Garzoli, S. L.: Meridional Overturning Circulation transport variability at 34.5° S during 2009-2017: Baroclinic and barotropic flows and the dueling influence of the boundaries, Geophys. Res. Lett., 45(9), 4180-4188, doi: 10.1029/2018GL077408, 2018.

Philander, S. G. H., and Pacanowski, R. C.: A model of the seasonal cycle in the tropical Atlantic Ocean, J. Geophys. Res., 91 (C12), 14192–14206, doi:10.1029/JC091iC12p14192, 1986.

Polo, I., Lazar, A., Rodriguez-Fonseca, B., and Arnault, S.: Oceanic Kelvin waves and tropical Atlantic intraseasonal variability: 1. Kelvin wave characterization, J. Geophys. Res., 113, C07009, doi:10.1029/2007JC004495, 2008.

Pujol M.-I., Faugère, Y., Taburet, G., Dupuy, S., Pelloquin, C., Ablain, M., and Picot, N.: DUACS DT 2014: the new multimission altimeter dataset reprocessed over 20 years, Ocean Sci. Discuss., doi:10.5194/os-2015-110, 2016.

Richardson, P. L.: On the history of meridional overturning circulation schematic diagrams. Prog. Oceanogr., 76, 466–486. doi:10.1016/j.pocean.2008.01.005, 2008.

Rodrigues, R. R., Rothstein, L. M., and Wimbush, M.: Seasonal Variability of the South Equatorial Current Bifurcation in the Atlantic Ocean: A Numerical Study. J. Phys. Oceanogr., 37, 16–30, doi:10.1175/JPO2983.1, 2007.

Roessler, A., Rhein, M., Kieke, D., and Mertens, C.: Long-term observations of North Atlantic Current transport at the gateway between western and eastern Atlantic. J. Geophys. Res.-Oceans, 120,4003–4027. doi:10.1002/2014JC010662, 2015.

Rühs, S., Getzlaff, K., Durgadoo, J. V., Biastoch, A., Böning, C. W.: On the suitability of North Brazil current transport estimates for monitoring basin-scale AMOC changes. Geophys. Res. Lett., 42, 8072–8080, 2015.

Schmidtko, S., and Johnson, G. C.: Multidecadal warming and shoaling of Antarctic Intermediate Water, J. Clim., 25(1), 207–221, 2012.

Schott, F. A., Dengler, M., Zantopp, R., Stramma, L., Fischer, J., and Brandt, P.: The Shallow and Deep Western Boundary Circulation of the South Atlantic at 5° –11° S. J. Phys. Oceanogr., doi:10.1175/JPO2813.1, 2005.

Send, U., Lankhorst, M., and Kanzow, T.: Observation of decadal change in the Atlantic meridional overturning circulation using 10 years of continuous transport data. Geophys. Res. Lett., doi:10. 1029/2011GL049801, 2011.

Silva, M., Araujo, M., Servain, J., Penven, P., and Lentini, C.A.D.: High-resolution regional ocean dynamics simulation in the southwestern tropical Atlantic. Ocean Model. 30, 256–269. https://doi.org/10.1016/j.ocemod.2009.07.002, 2009.

Silveira, I. C. A. d., Miranda, L. B., and Brown, W. S.: On the origins of the North Brazil Current, J. Geophys. Res., 99, 22501-22512, 1994.

Srokosz, M. A., and Bryden, H. L.: Observing the Atlantic meridional overturning circulation yields a decade of inevitable surprises, Science 348, 1255575, doi:10.1126/science.1255575, 2015.

Talley, L. D. (2003). Shallow, intermediate and deep overturning componentsof the global heat budget. J. Phys. Oceanogr., 33, 530–560, 2003.

Toole, J. M., Andres, M., Le Bras, I. A., Joyce, T. M., and McCartney, M. S.: Moored observations of the deep western boundary current in the NW Atlantic: 2004–2014. J. Geophys. Res.-Oceans 122, 7488–7505. doi:10.1002/2017JC012984, 2017.

Watts, D. R., and Kontoyiannis, H.: Deep-ocean bottom pressure measurement—Drift removal and performance. J. Atmos. Ocean. Tech., 7(2), 296–306, 1990.

Worthington, E. L., Frajka-Williams, E., and McCarthy, G. D.: Estimating the deep overturning transport variability at 26° N using bottom pressure recorders. J. Geoph. Res. Oceans, 124, 335– 348. doi:10.1029/2018JC014221, 2019.

Zantopp, R., Fischer, J., Visbeck, M., and Karstensen, J.: From interannual to decadal: 17 years of boundary current transports at the exit of the Labrador Sea. J. Geophys. Res. Oceans, 122, 1724–1748. doi:10.1002/2016JC012271, 2017.

Zhang, D., Msadek, R., McPhaden, M. J., and Delworth, T.: Multidecadal variability of the North Brazil Current and its connection to the Atlantic meridional overturning circulation, J. Geophys. Res., 116, C04012, 2011.

Zhao, J., and Johns, W. E.: Wind-forced interannual variability of the Atlantic Meridional Overturning Circulation at 26.5° N, J. Geophys. Res. Oceans, 119, 2403– 2419, doi:10.1002/2013JC009407, 2014.

Acronym	Mooring ID	Instrument	Position	Depth	Deployment period
$P_{WB\ 500m\ a}$	KPO 1109	PIES	10.2367°S 35.8633°W	500m	05/2013 - 10/2015
$P_{EB\ 300m}$	KPO 1110	Single SBE 26plus sensor	10.6830°S 13.2250°E	300m	07/2013 - 11/2015
$P_{EB\ 500m}$	KPO 1106	ADCP shield with SBE 26plus sensor	10.7090°S 13.1855°E	500m	07/2013 - 10/2015
$P_{WB\ 300m}$	KPO 1134	PIES	10.2320°S 35.8780°W	300m	05/2014 - 09/2016 09/2016 - 03/2018*
$P_{WB\ 500m\ b}$	KPO 1135	PIES	10.2430°S 35.8700°W	500m	05/2014 - 09/2016 09/2016 - 02/2018*

Table 1 Collection of available BP measurements at 11° S. Acronyms used throughout this article are given in the 1st column, official mooring IDs and instrument types are listed in the 2nd and 3rd columns. Columns 4-6 give the positions, depths and deployment periods for each BP measurement. The BP data can be found at https://doi.pangaea.de/10.1594/ PANGAEA.907589.

***These sensors were re-deployed in 2018 and are currently in place.**

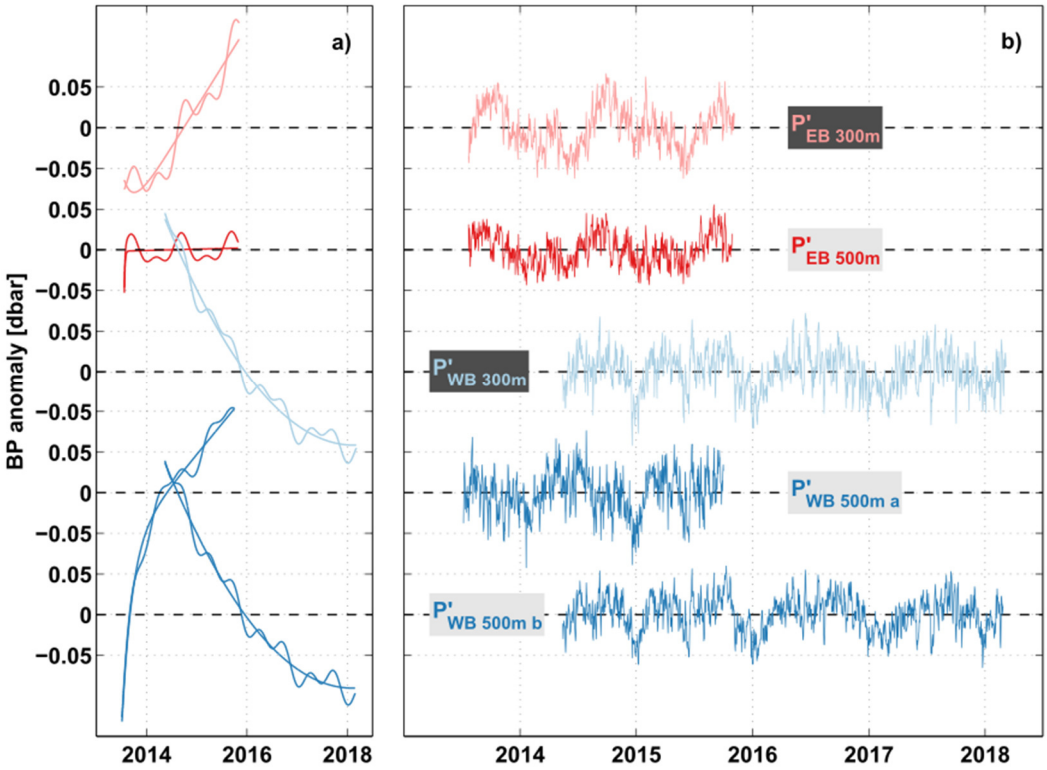

Figure 1 ~~**Time series of**~~ **Bottom pressure (BP) anomalies measured at 11° S off Angola at 300 m (pink) and 500 m (red), as well as off Brazil at 300 m (light blue) and 500 m (blue) depth. a) Instrument drifts that are removed from** ~~**the individual BP anomaly time series shown in b)**~~**, as well as the sum of the drift and the combined annual and semi-annual harmonics fitted to the individual BP anomaly time series. b) Daily time series of BP anomalies after** ~~**handling,**~~ **de-tiding and de-drifting (see text for details).**

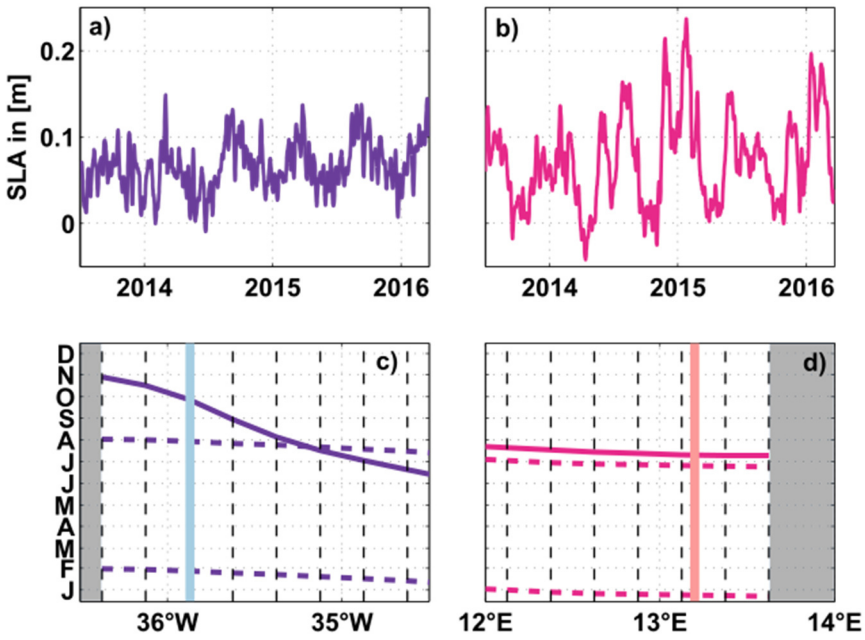

820 **Figure 2 ~~(a,b)~~ Time series of SLA over the period 2013-2018 – chosen close to the western ~~boundary~~ (purple; a) and eastern ~~boundary~~ boundaries (magenta; b). ~~(c, d)~~ Phases of the minima of the annual (solid curve) and semi-annual (dashed curves) harmonics as function of longitude near the western (c) and eastern (d) boundaries. In (c, d), the b~~B~~lack dashed lines represent the zonal grid spacing of the SLA data and grey areas mark land. Light blue (c) and ~~(~~pink (d)~~)~~ lines mark the locations of the 300 m BPRs at the western (c) and eastern (d) boundaries.~~the western (eastern) boundary. Gray areas mark land.~~**

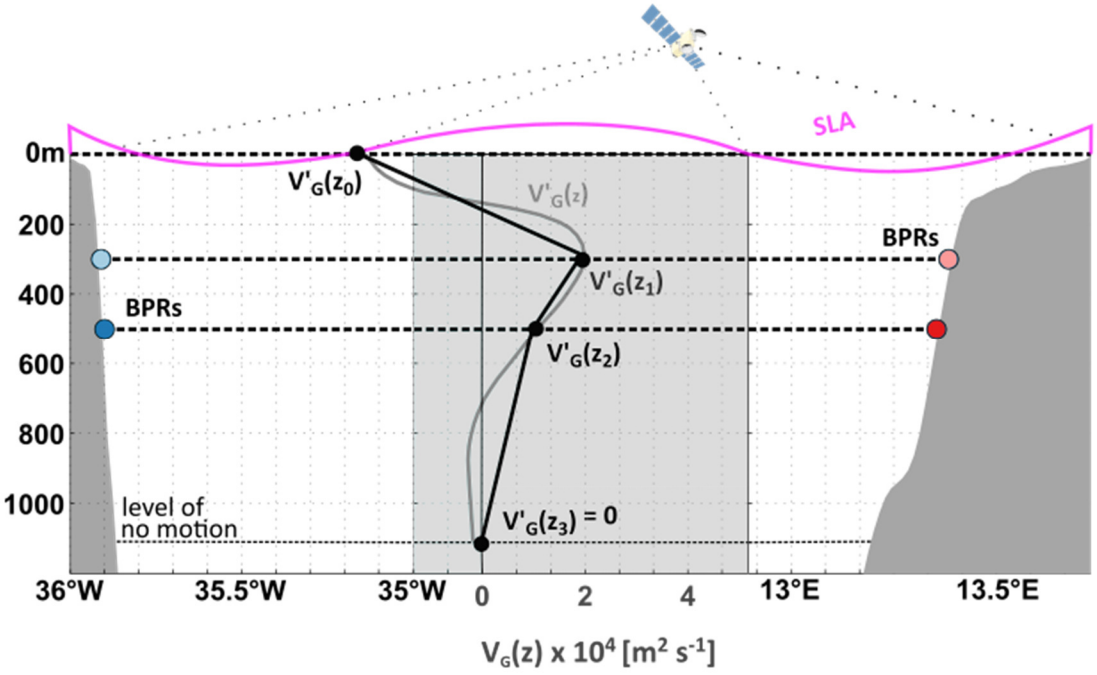

Figure 3 Experimental setup and strategy to estimate T'_G showing the location of the BPRs (reddish & blueish circles) and the vertical sampling of V'_G. V'_G is derived from measurements of sea level anomaly ~~, z_0=0 m,~~ and with ~~BPRs~~ bottom pressure at ~~two depth levels~~300 m and 500 m depth~~, z_1= 300 m and z_2= 500 m~~. A level of no motion is prescribed to be at z_3=-1130 m. Two methods are used t~~T~~o approximate $V'_G(z)$ ~~two methods are used~~: i) piecewise linear interpolation of V'_G between the 4 data points (black profile), ii) regression of the 1st and 2nd dominant vertical structure functions of $V'_{G\,SIM\,P(z)}$ from INALT01 onto the data points at 0 m, 300 m and 500 m depth relaxing the no-flow condition at 1130 m depth (grey profile). $V'_G(z)$ is then vertically integrated from 1130 m to the surface to derive T'_G.

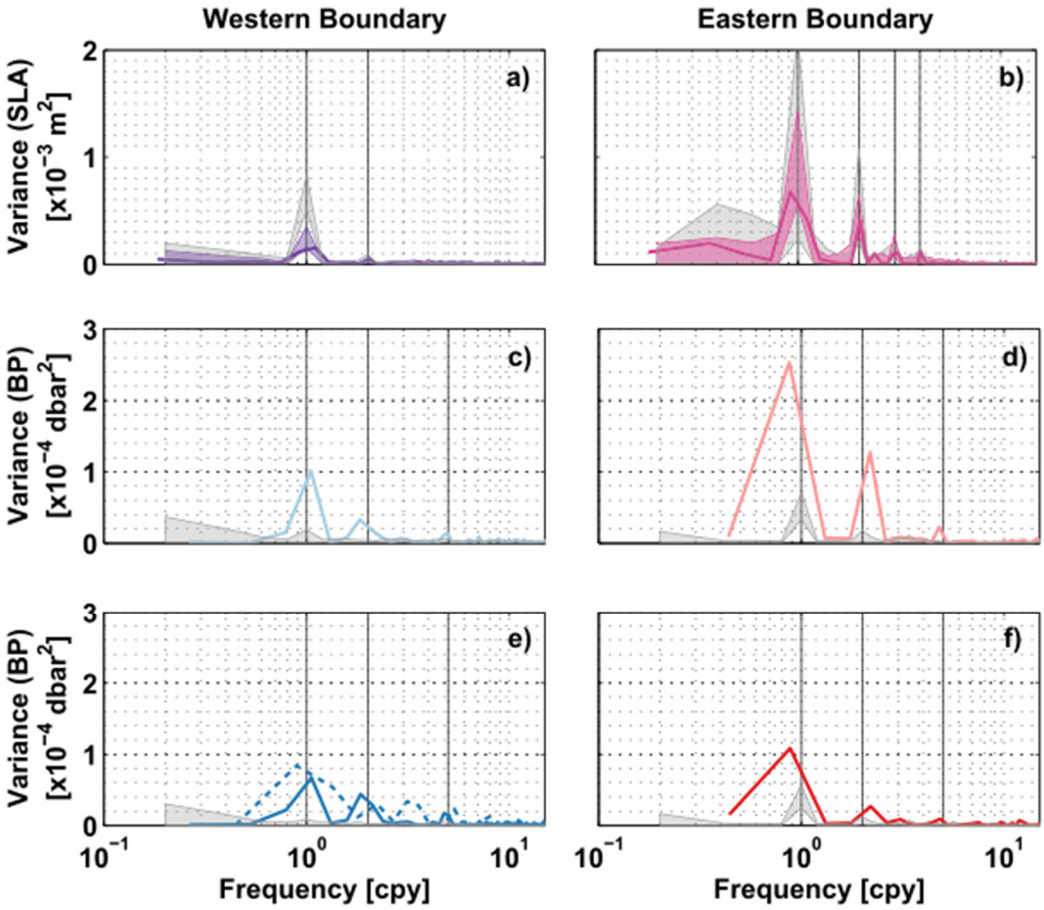

Figure 4 Periodograms of (a, b) SLA, (c, d) BP at 300 m and (e, f) BP at 500 m depth –from observations (colored), and from the INALT01 model (grey). In (a, b) bold solid curves show periodograms calculated from SLA data over the period 2013-2018. The transparent envelopes are an estimate for interannual variations, specifically, the minimum and maximum ranges of periodograms calculated for 5-year windows running through the full available period 1993-2018. In (c, f) bold solid curves show periodograms calculated from the individual BP time series available at 11°S. In e) the solid curve represents KPO 1135 and the dashed curve KPO 1109 (two co-located sensors covering different periods; see Table 1). Grey shading in all panels gives the minimum and maximum ranges of periodograms for SLA and BP time series derived from the INALT01 model calculated for 5-year windows running through the full available period 1978-2007. Frequency is given in 'cycles per year'. Black vertical lines mark the frequencies of the annual and semi-annual cycles, as well as periods of 120 and 90 days in (b) or 70 days in (c, d, e, f).

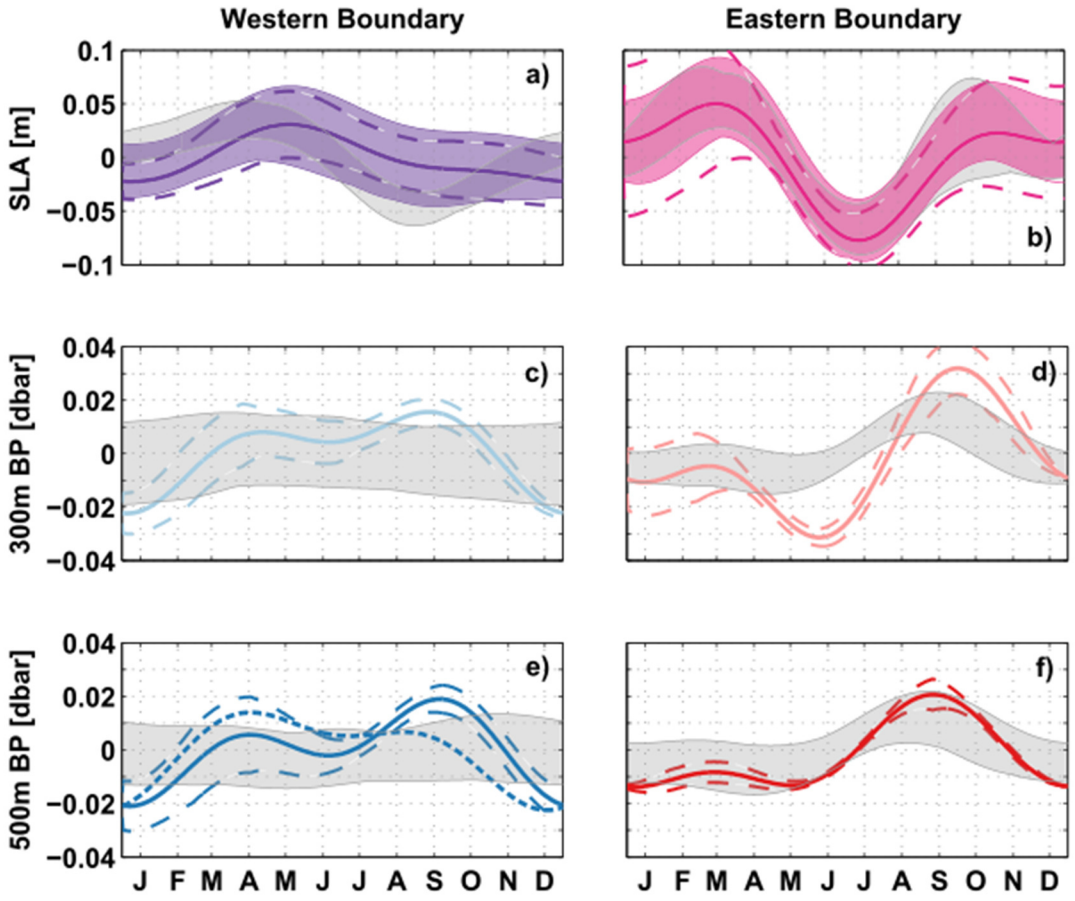

Figure 5 Combined annual and semi-annual harmonics calculated for (a-b) SLA, (c-d) BP at 300 m and (e-f) BP at 500 m depth. Line styles and color coding are the same as in Fig. 4. Additionally, dashed ~~lines and curves~~envelopes around the solid curves give uncertainties for the amplitudes of the harmonics. These are calculated by 170-days low-pass filtering the pressure time series and then subsequently the 95th percentile of the deviations from the derived annual and semi-annual harmonics for every day of the year ~~calculated as described in section 4.1~~.

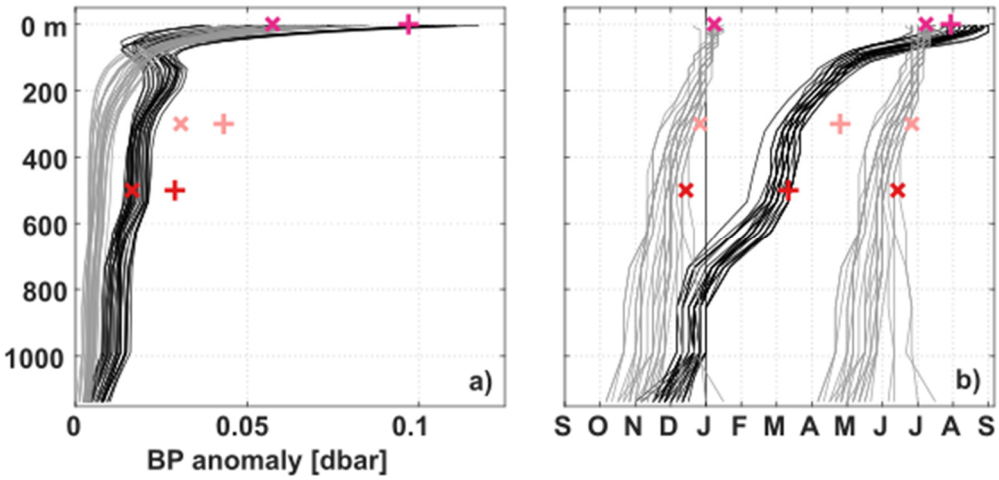

Figure 6 (a) Amplitudes and (b) phases of the minima of the annual (pluses and black curves) and semi-annual (crosses and grey curves) harmonics of the pressure anomalies at the eastern boundary along 11° S. Markers represent estimates ~~–~~from the observations (2013-2018) at 0m ~~(magenta)~~, at 300m ~~(pink)~~, 500m ~~(red)~~, ~~-~~the curves show estimates calculated from INALT01 for 5-year windows running through the period of available data (1978-2007).

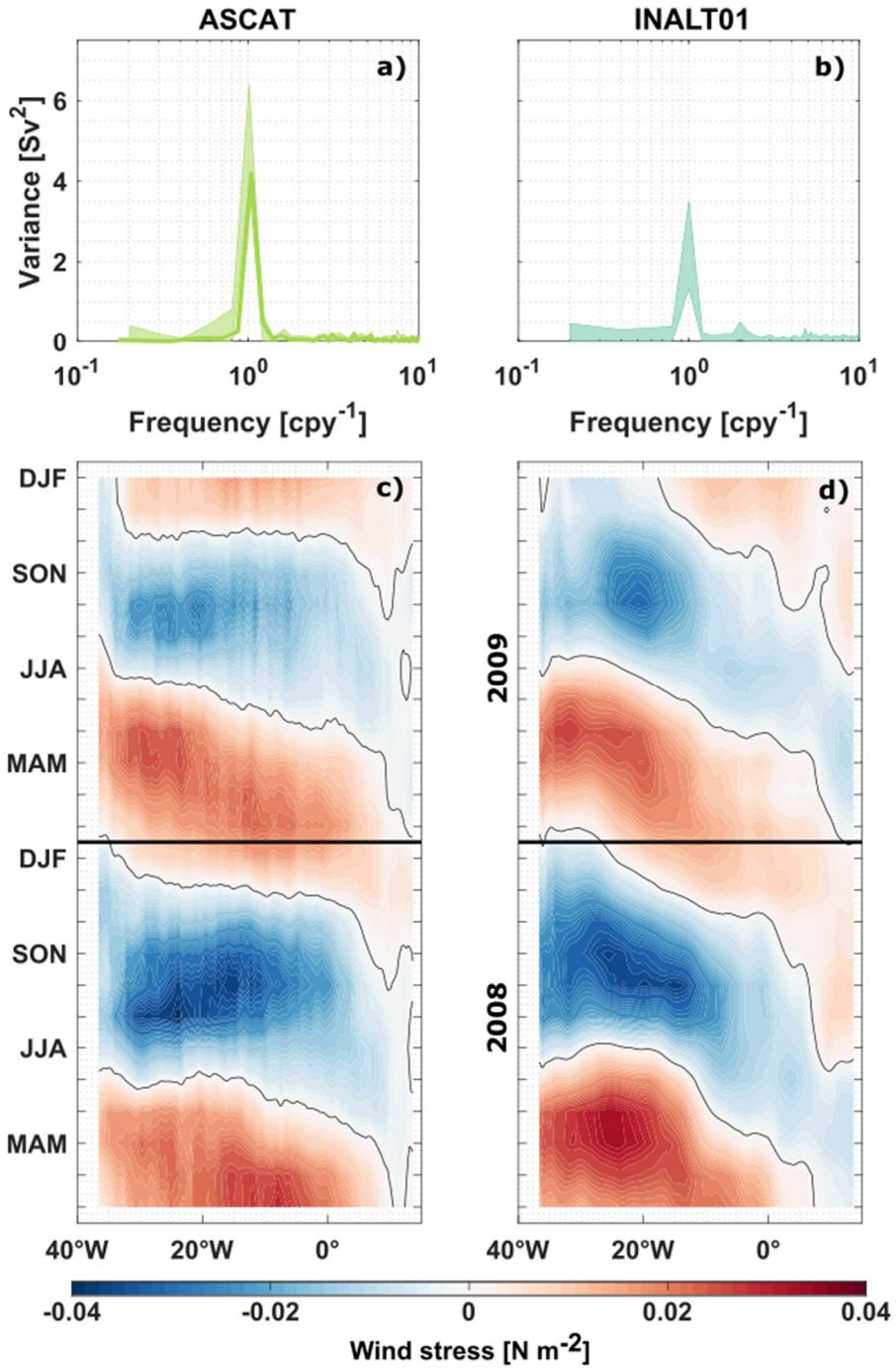

Figure 7 (a-, b) Periodograms of the Ekman transport at 11° S, derived from ASCAT (a) and INALT01 (b) wind stress. The Bbold curve in (a)s are is calculated for the period 2013-2018.ASCAT (left panels) over the period 2013-2018 and for CORE2b (right panels) over 2002-2007. Thin curves ransparent envelopes in (a-b) give an estimate for interannual variations, give specifically the minimum and maximum ranges of periodograms calculated for 5-year windows running through the full available time series of

ASCAT (2008-2018) and INALT01 (1978-2009). ~~1993-2018 for ASCAT and 1978-2009 for CORE2b.~~ Frequency is given in 'cycles per year'. (c-d) ~~Hovmoeller~~ Hovmöller diagrams of the ASCAT (c) and INALT01 (d)~~CORE2b~~ zonal wind stress anomalies along 11° S for the overlapping years 2008-2009. Red (blue) colors in (c, d) imply eastward (westward) wind stress anomalies.

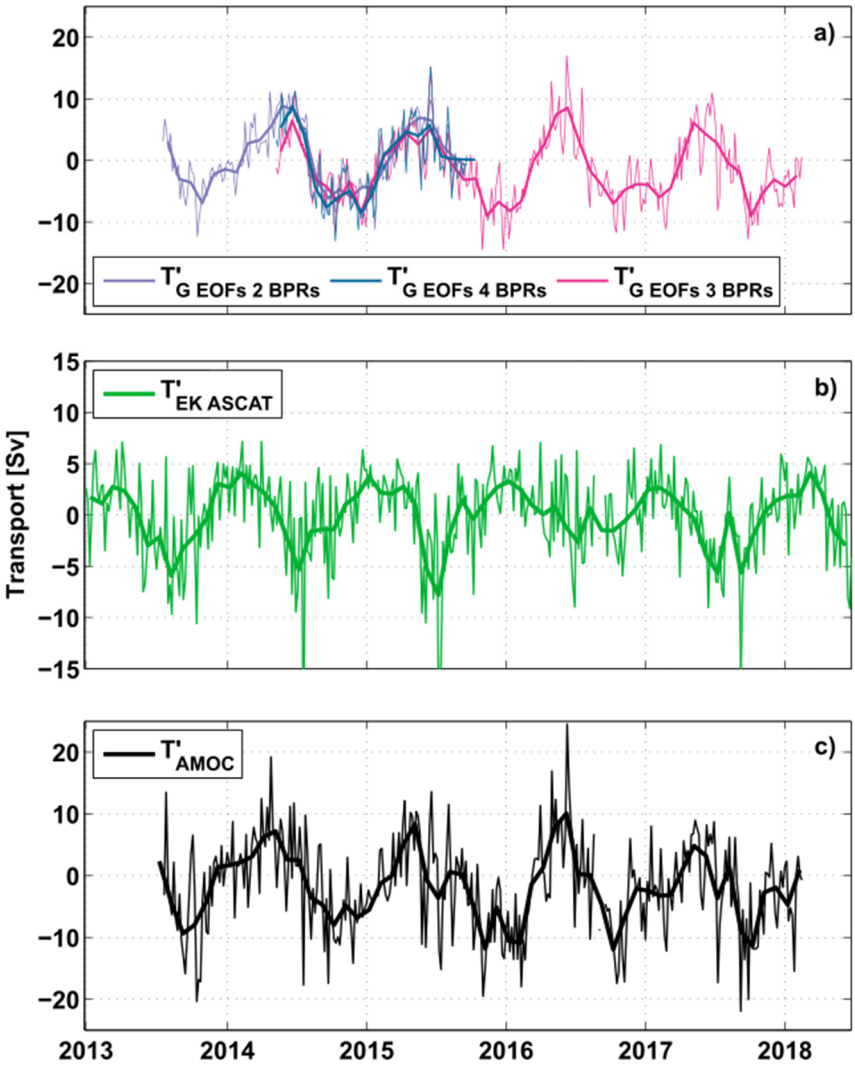

Figure 8 Anomaly time series at 11° S of ~~(daily in a) and 5-daily in (b-c) as thin lines, and monthly averages as bold lines) of~~ (a) the upper-ocean geostrophic transport ($T'_{G\ EOFs}$), (b) the Ekman transport derived from ASCAT wind stress ($T'_{EK\ ASCAT}$~~; green~~), and (c) the resulting AMOC transport (T'_{AMOC}~~; black~~). Thin lines represent daily values in a) and 5-daily values in (b, c), bold curves represent monthly averages. Different colors in ~~the upper panel~~(a) indicate transport calculations for different sets of BPRs – 4 BPRs (petrol), 3 BPRs (500 m WB, 300 m EB, 500 m EB; purple) and 2 BPRs (300 m & 500 m WB; magenta) combined with the annual and semi-annual harmonics derived from the fully equipped period (05/2014-10/2015; see section 4.1).

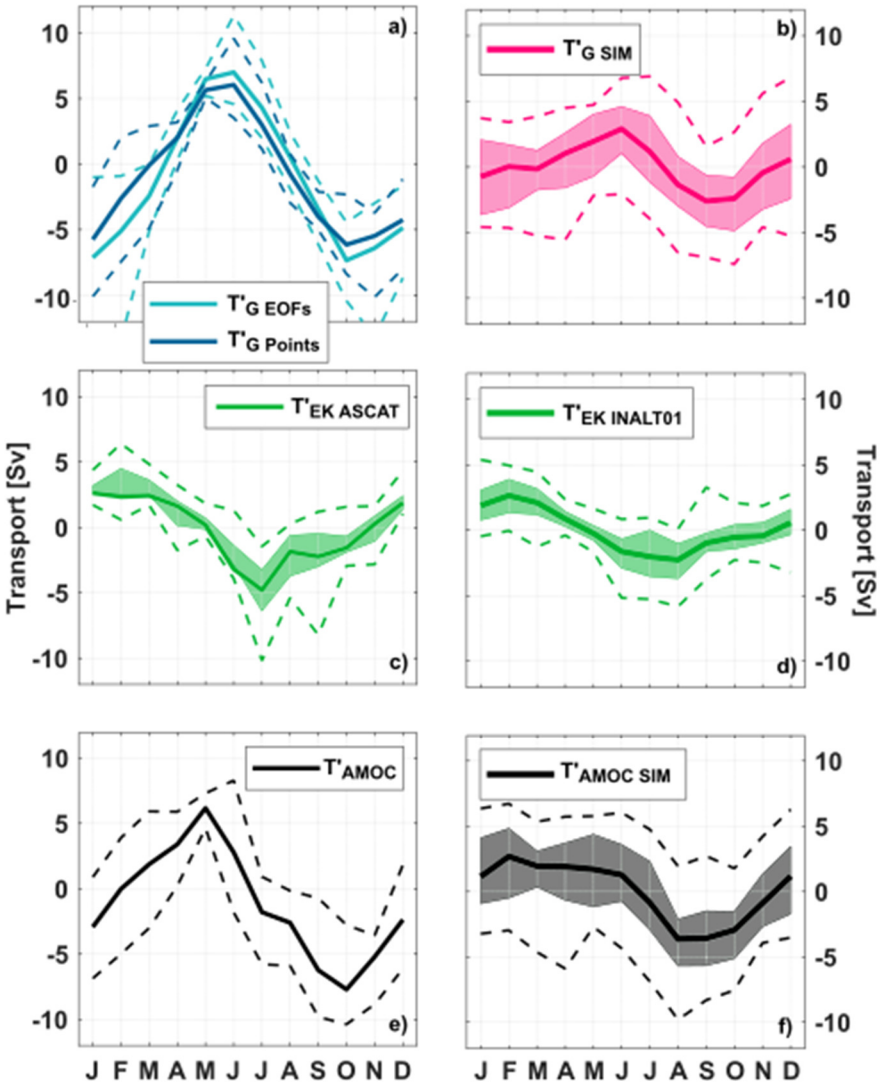

Figure 9 Mean seasonal cycles of ~~transport anomalies~~ T'_G (a, b), T'_{EK}.(c, d) and, T'_{AMOC} (e, f) from observations (a, c, e) and the INALT01 model (b, d, f). Upper-ocean geostrophic transport anomalies, $T'_{G\ Points}$ (petrol curve) and $T'_{G\ EOFs}$ (~~teal~~ cyan curve), are derived from SLA and BP observations (as described in section 4.1) and averaged over the period 2013-2018, while $T'_{G\ SIM}$, is derived from the INALT01 model velocity fields (as described in section 4.2) and averaged over the period 1978-2007. ~~For the observations, the respective standard errors per month are given by the error bars.~~ T'_{AMOC} in (e) was derived using $T'_{G\ EOFs}$. For the 30-year INALT01 run (b,d,f) and the 12-year ASCAT wind time series (c), ~~shading~~ transparent envelopes represent~~s~~ an estimate for interannual variations, specifically, the minimum and maximum range of mean seasonal cycles calculated for ~~running~~ 5-year windows running through the respective available periods~~, representing interannual variability~~. The dashed curves in all panels show the absolute range of possible minima and maxima per months.

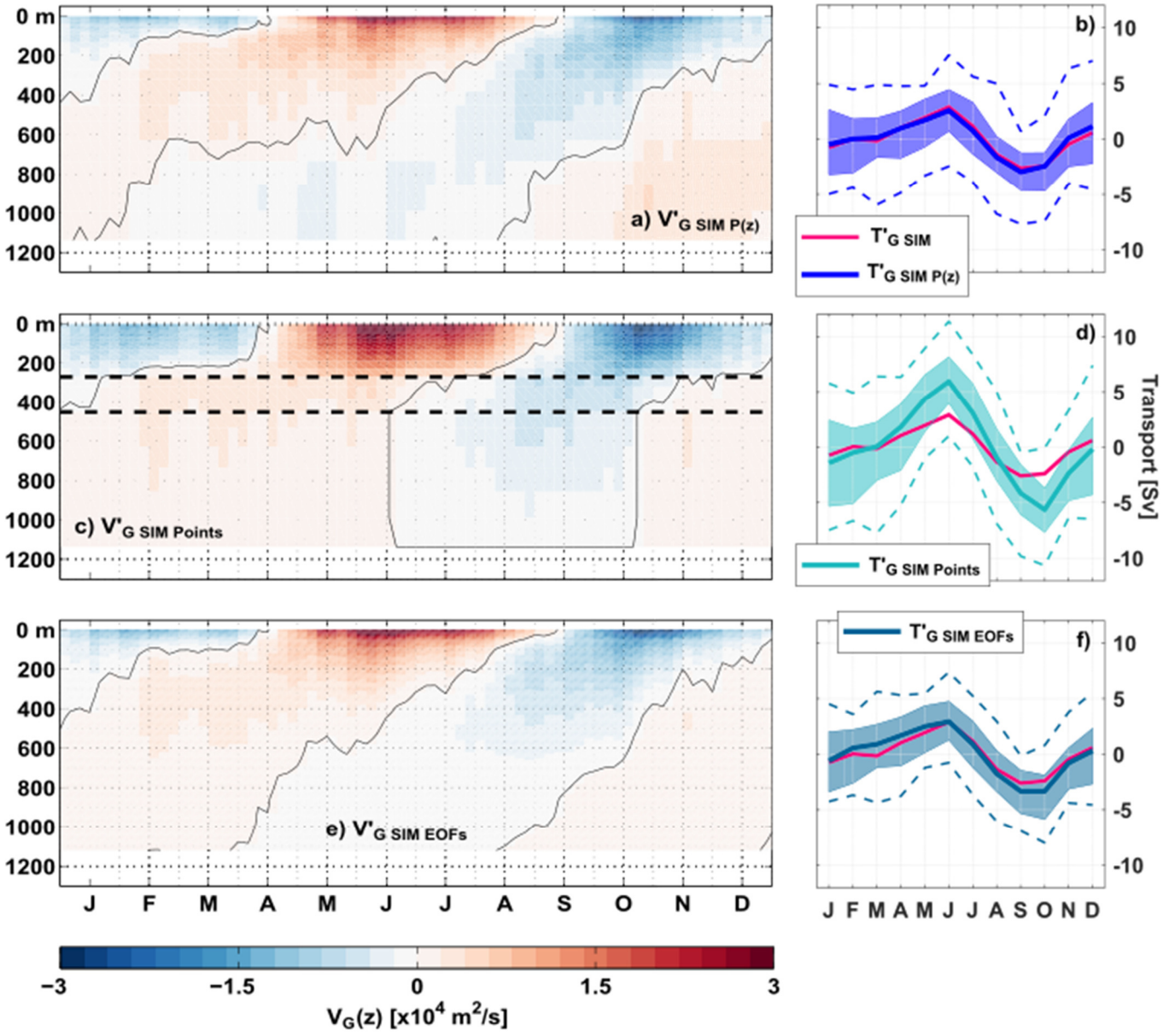

Figure 10 Mean seasonal cycles of the geostrophic transport per unit depth, $V'_{G\,SIM}$ (a,c,e) and the upper-ocean geostrophic transport $T'_{G\,SIM}$ (pink curves; b, d, f) from INALT01. $V'_{G\,SIM\,P(z)}$ (a) and $T'_{G\,SIM\,P(z)}$ (~~cyan~~ blue curve; b), were calculated using the full vertical profiles of BP. $V'_{G\,SIM\,Points}$ (c) and $T'_{G\,SIM\,Points}$ (~~petrol~~ cyan curve; d) were reconstructed by piecewise linear interpolation of V'_G between the 4 supporting points at 0, 300, 500, and 1130 m depth (black dashed lines in c) mark the depths of the BPRs); $V'_{G\,SIM\,EOFs}$ (e) and $T'_{G\,SIM\,EOFs}$ (petrol~~teak~~ curve; f) by using the dominant vertical structure functions from INALT01. In (a, c, e) red (blue) colors show ~~positive (~~northward~~) and blue colors negative~~ (southward) anomalies. ~~Blue curves in (b,d,f) represent the seasonal cycle of $T'_{G\,SIM}$ derived from the INALT01 model velocity fields (as described in section 4.2). The shading in (b,d,f) represents the minimum and maximum range of mean seasonal cycles calculated for running 5-year windows of the 30-year model run.~~

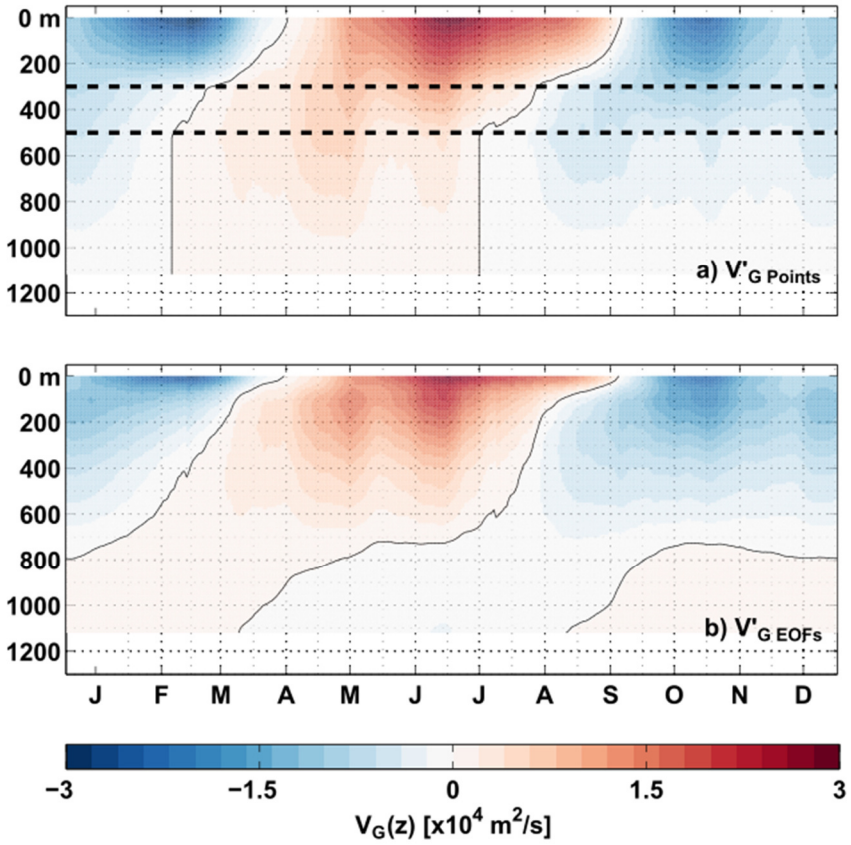

Figure 11 Mean seasonal cycle of the geostrophic transport per unit depth, V'_G, over the period 2013-2018, derived from observations at 11° S with two methods: (a) Piecewise linear interpolation between the 4 supporting points at 0, 300, 500 and 1130 m depth (black dashed lines mark the depths of the BPRs). (b) Reconstruction of V'_G by regression of the dominant vertical structure functions from the INALT01 model onto the values at the 3 depth levels of pressure observations at 0 m, 300 m, 500 m depth thereby relaxing the no-flow condition at 1130 m depth. Red (blue) colors show ~~positive (~~northward~~) and blue colors negative~~ (southward) anomalies.

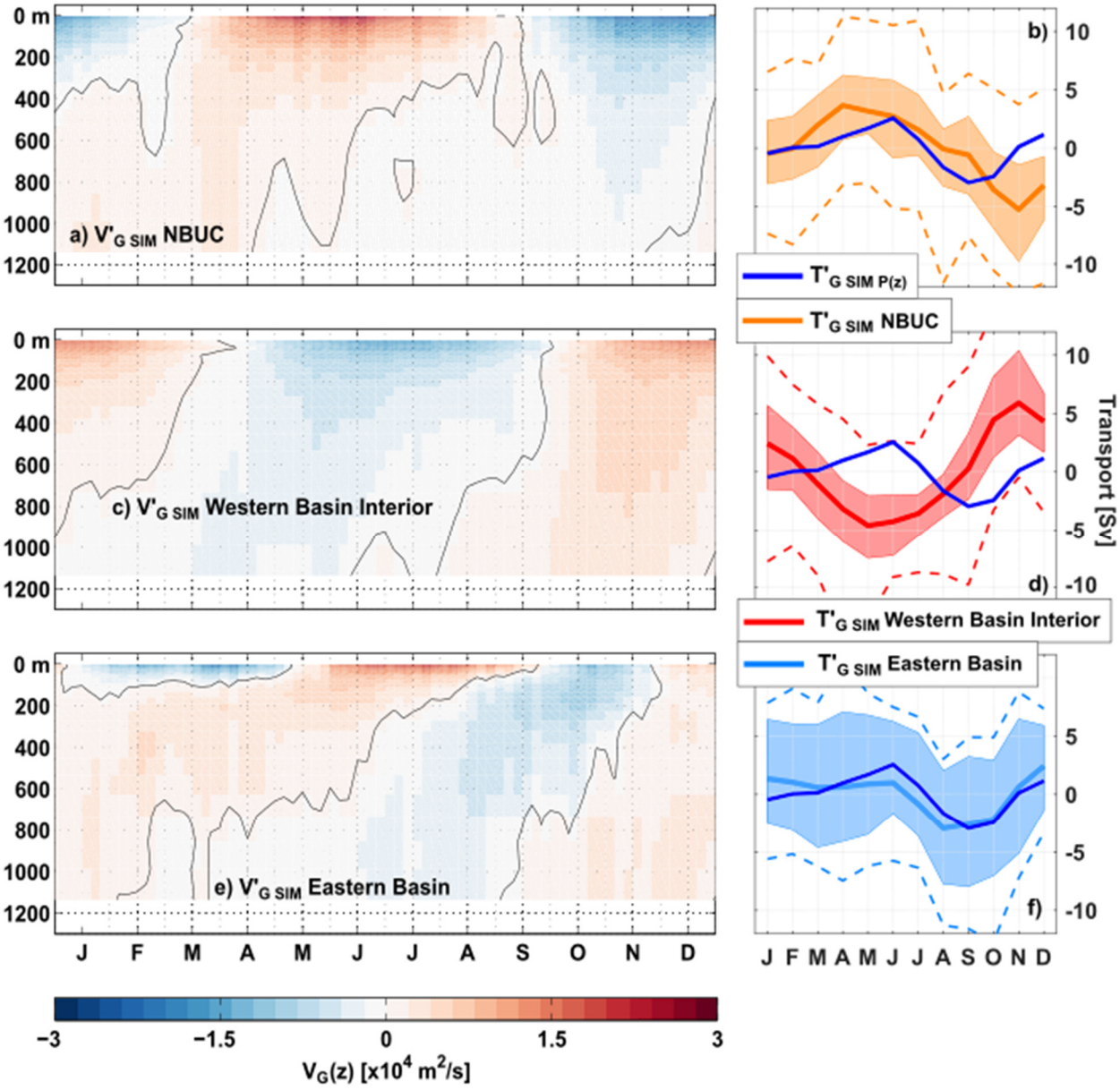

Figure 12 Mean seasonal cycle of the geostrophic transport per unit depth, $V'_{G\,SIM}$ (a,c,e) and the upper-ocean geostrophic transport $T'_{G\,SIM}$ (b,d,f) from INALT01. In all panels, V'_G and T'_G were calculated from the full vertical profiles (from the surface down to 1130 m) of the simulated pressure, but from pressure differences across different regions along 11° S: across the whole basin ($T'_{G\,SIM\,P(z)}$; ~~cyan~~ blue curves in b, d, f); between the Brazilian continental slope and 34.55° W ($V'_{G\,SIM}$ $NBUC$ in a; $T'_{G\,SIM}$ $NBUC$ orange curves in b); between 34.55° W and 10~~5~~° W ($V'_{G\,SIM}$ $Western\ Basin\ Interior$ in c; $T'_{G\,SIM}$ $Western\ Basin\ Interior$ red curves in d); between ~~5~~10° W and the Angolan continental slope ($V'_{G\,SIM}$ $Eastern\ Basin$ in e; $T'_{G\,SIM}$ $Eastern\ Basin$ light blue curve in f). Transparent shading and dashed curves are the same as in Fig. 9.~~Line styles and color coding is the same as for Fig. 10.~~

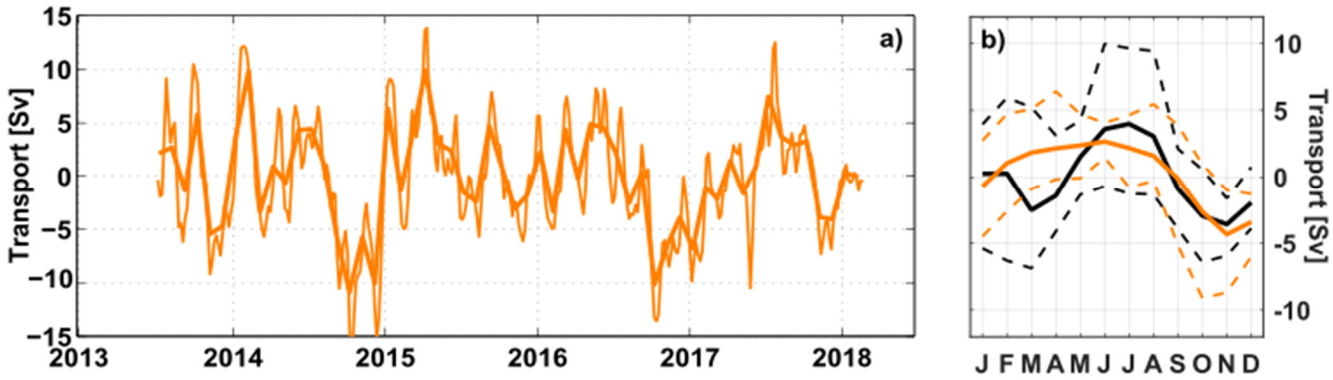

Figure 13 a) Time series of NBUC transport anomalies (5-daily as thin curve, and monthly averages as bold curve) based on moored observations off Brazil (see section 2.4) updated from Schott et al. (2005) and Hummels et al. (2015). b) Mean seasonal cycles of the NBUC transport anomalies averaged over the periods 2013-2018 (~~bold~~ orange curve) and 2000-2004 (~~thin dashed~~black curve). ~~The respective standard errors per month are given by the error bars.~~ The thin dashed curves show the absolute range of possible minima and maxima per months for the periods 2013-2018 (orange) and 2000-2004 (black), respectively.

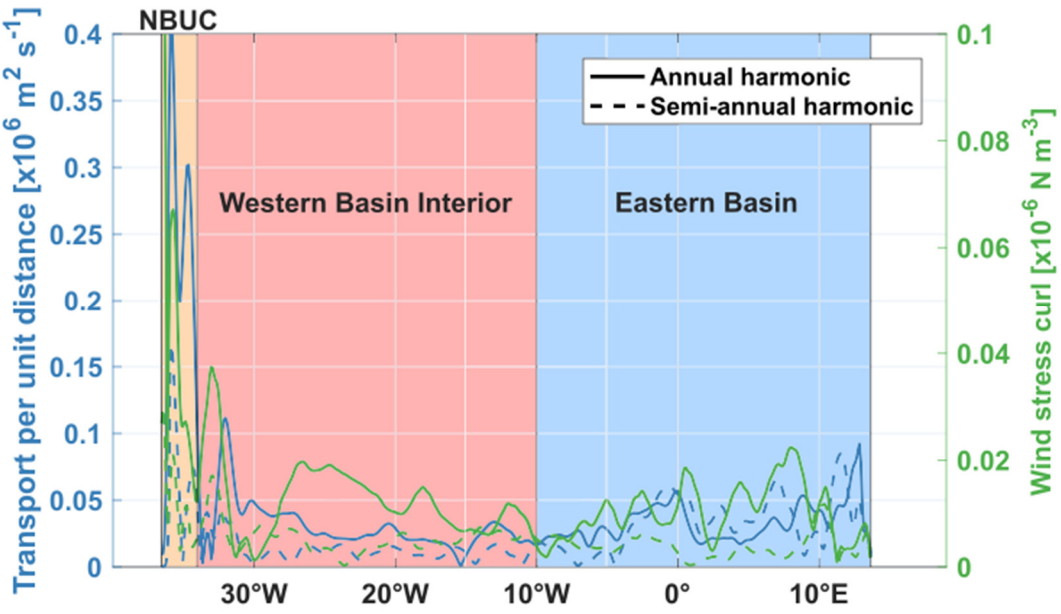

Figure 14 a) Amplitudes of the annual (solid curves) and semi-annual (~~dotted~~ dashed curves) harmonics of the vertically integrated upper-ocean geostrophic velocity in INALT01 (blue curves; left axis) and the INALT01 wind stress curl (green curves, right axis) ~~– both from INALT01 –~~ along 11° S. Transparently shaded boxes highlight different ~~regimes~~ regions – the NBUC (orange), the western basin interior (red) and the eastern basin (blue). ~~b) Zonal section of the phase of the annual harmonic of the meridional velocity in INALT01 along 11° S. White hatching overlays part of the section, where the harmonics have an amplitude < 0.0025 m/s. The white line marks the assumed level of no motion at 1130 m. c) Same as b), but for the semi-annual harmonic of the meridional velocity.~~